NASA CONTRACTOR REPORT

NASA CR-392

NASA CR-39

MOLECULAR OXYGEN DENSITIES FROM ROCKET MEASUREMENTS OF LYMAN-α ABSORPTION PROFILES

by Leslie G. Smith and Lawrence Weeks

Prepared under Contract No. NASw-820 *by*
GCA CORPORATION
Bedford, Mass.
for

NATIONAL AERONAUTICS AND SPACE ADMINISTRATION • WASHINGTON, D. C. • MARCH 1966

MOLECULAR OXYGEN DENSITIES FROM ROCKET MEASUREMENTS OF LYMAN-α ABSORPTION PROFILES

By Leslie G. Smith and Lawrence Weeks

Prepared under Contract No. NASw-820 by
GCA CORPORATION
Bedford, Mass.

for

NATIONAL AERONAUTICS AND SPACE ADMINISTRATION

For sale by the Clearinghouse for Federal Scientific and Technical Information
Springfield, Virginia 22151 – Price $3.00

ACKNOWLEDGEMENTS

The work described in this report was conducted as part of two projects for the National Aeronautics and Space Administration, under contracts NASw-500 and NASw-820. Many people contributed to the several aspects of the program. P. J. McKinnon and S. A. Sapuppo made valuable contributions with respect to the payload instrumentation. R. V. Sillars and K. W. Anderson assisted with the data analysis.

ABSTRACT

This report contains a description of the measurement of molecular oxygen in the upper atmosphere by absorption spectroscopy using solar Lyman-α radiation. The experimental arrangement used in the payloads of Nike Apache rockets and the method of analysis are detailed. Data from rocket flights at Wallops Island, Virginia, and Fort Churchill, Manitoba, for the altitude range 70 to 112 km are presented. Conclusions are drawn from this and other data obtained by absorption spectroscopy.

TABLE OF CONTENTS

NOMENCLATURE

F	optical depth factor
$\mathcal{F}$	$= \frac{H^{\frac{1}{2}}F}{101.4}$
h	minimum ray height; hour angle
H	density scale height
I	radiation flux at rocket; ion chamber current
I_o	radiation flux incident on the atmosphere
$I(0)$	ion chamber current for zero aspect angle
$I(\alpha)$	ion chamber current for aspect angle α
n	particle number density; index of refraction
n_T	columnar particle density
R	radius of the Earth
s	distance along ray
S	ion chamber sensitivity at Lyman-α
T	fraction of radiation transmitted by ion chamber window
u	$= (x/H)^{\frac{1}{2}}$
x	altitude above minimum ray height
z	altitude of rocket
α	aspect angle of ion chamber; right ascention
δ	declination
δh	uncertainty in minimum ray height
δn	uncertainty in number density
$\delta\chi$	uncertainty in zenith angle
φ	latitude of sub-rocket point
σ	absorption cross section
χ	solar zenith angle

MOLECULAR OXYGEN DENSITIES FROM ROCKET MEASUREMENTS OF LYMAN-α ABSORPTION PROFILES

By Leslie G. Smith and Lawrence Weeks

INTRODUCTION

The two basic methods for determining the concentration of different neutral species in the upper atmosphere are absorption spectroscopy and mass spectroscopy. At present, absorption spectroscopy is preferred for accurate quantitative determinations because the data interpretation is relatively unambiguous and straightforward. The accuracy of various mass spectrometric methods is compromised by effects associated with motion of the rocket (velocity and orientation) and reactions at the walls of the instrument.

Spectrographs, capable of measuring the absorption profile of solar radiation in a very narrow wavelength band, permit very accurate analyses of the pertinent constituents; however, much less costly instruments are sufficiently accurate for some applications. These include ion chambers, gas gain and proportional detectors, and Geiger counters. Of these, ion chambers permit the most accurate flux measurements, but they can only be used when the incident flux in the wavelength band to be measured is sufficiently high.

The operation of these detectors depends on ionization of the gas contained in them and the applied voltage. The long-wavelength limit is determined by the ionization threshold of the gas and the short-wavelength limit is set by the transmission characteristics of the window material. The detectors utilizing this principle that are presently available for rocket or satellite measurements provide various spectral bands from .1 to 60Å and 1050 to 1590Å [1]*.

A particular atmospheric constituent (or constituents) is selected by the choice of wavelength bands to be measured, and the absorption coefficient of the atmosphere at this wavelength then sets the height range for the measurements. The absorption of solar hydrogen Lyman-α is particularly useful for the measurement of the molecular oxygen concentration since molecular oxygen is the primary absorber and since suitable ion chambers are available. Although the response of the ion chamber for measuring Lyman-α radiation is several hundred angstroms wide, a virtually monochromatic response is achieved because of the large flux of Lyman-α compared with other wavelengths in the band pass and because these other wavelengths are removed by absorption at much greater altitudes.

*Numbers in [ ] throughout the text indicate reference numbers.

This report is based on experience with these detectors obtained on two sounding rocket programs for the National Aeronautics and Space Administration, both using Nike Apache rockets. During the solar eclipse of 20 July 1963, the primary purpose of the Lyman-α measurement was to observe the reduction in flux as the sun was eclipsed. The absorption profile of Lyman-α was also obtained and is included in this study. As part of the U.S. participation in the IQSY, these measurements are being made at more-or-less regular intervals during 1964 and in 1965. In these flights, the measurement of the molecular oxygen profile is the primary objective.

Features of the Lyman-α ion chambers and related instrumentation, as well as derivation of the formulae, method of data analysis, and an error discussion, pertinent to the measurement of molecular oxygen in the upper atmosphere, are given. The observations are presented and conclusions drawn from this and other data obtained by absorption spectroscopy.

INSTRUMENTATION

A cross-section of the ion chamber is shown in Figure 1 [2]. The ceramic housing of alumina, is plated with gold on the inside of the cylindrical section to minimize photo-electric emission and to exclude chemical reaction with the gas. A kovar connector, which also serves as a guard ring, prevents electrical leakage across the surface of the ceramic to the central electrode, also of kovar. A copper tube connected to the outer electrode (the gold plated inner surface) is used during fabrication to introduce the gas into the chamber. The ion chambers used in the rocket flights described here were manufactured in accord with the detailed description given by Stober [2].

The experimental arrangement is designed for a spin-stabilized sounding rocket system in which the ion chamber is fixed in relation to the rest of the payload. Although a minimum spin rate of 3 rps is needed for an adequate sampling rate, a value of 6 rps has generally been required for adequate spin stabilization of the Nike Apache rockets. The modulation of the signal produced by the rotation of the payload makes slow drift of the electrometer and amplifier unimportant (within certain limits).

The ion chamber is positioned in the payload so as to be in the most favorable position to view the sun for a particular flight. A typical arrangement is shown in Figure 2. A solar aspect sensor, directly below the ion chamber, provides data on the angle at which the ion chamber views the sun (aspect angle) [3]. This permits the measured ion chamber response to be corrected for its efficiency change with the angle of view. Both instruments are protected by doors during rocket ascent, which are released at an altitude of about 55 km.

Figures 3 and 4 show a block diagram and a schematic of the electronics used in the measurement of ion chamber current. The outer cylinder of the ion chamber is biased at +45 volts with respect to the center pin, and the positive current is fed to the electrometer. Since the output of the feedback electrometer amplifier (low gain output) is negative for a positive input signal, a subcarrier oscillator with a non-standard input range of 0 to -5 volt is used. The electrometer is designed for a maximum ion chamber current of 5×10^{-9} amps. This current produces a -5 volt output from the feedback electrometer amplifier, and this is fed directly to the telemetry system.

Small signals are further amplified by a factor of 25 and ac coupled to another channel in the telemetry system. The amplifier provides phase reversal so that a subcarrier oscillator of the standard input range 0 to 5 volts may be used. The system is ac coupled to the telemetry system through a capacitor to eliminate slow drift, and the signal is dc restored by a diode.

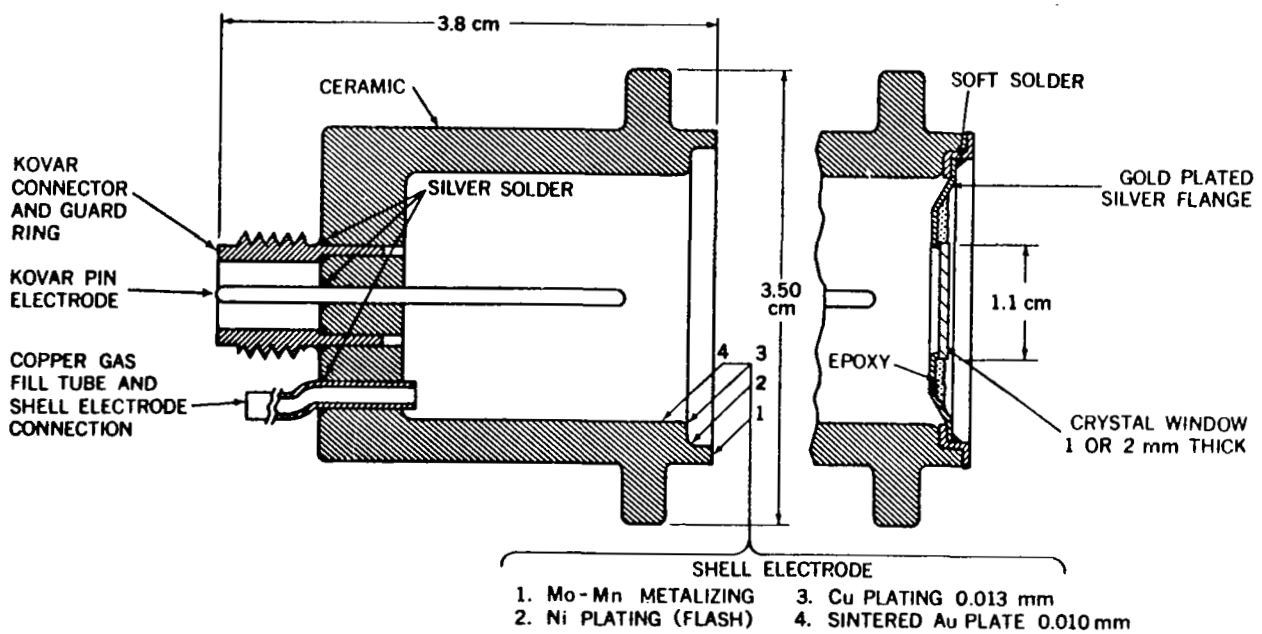

Figure 1. Cross section of the ion chamber. The inside diameter is 1.9 cm and length 2.3 cm. Window materials are generally of LiF, CaF_2 or BaF_2 crystals.

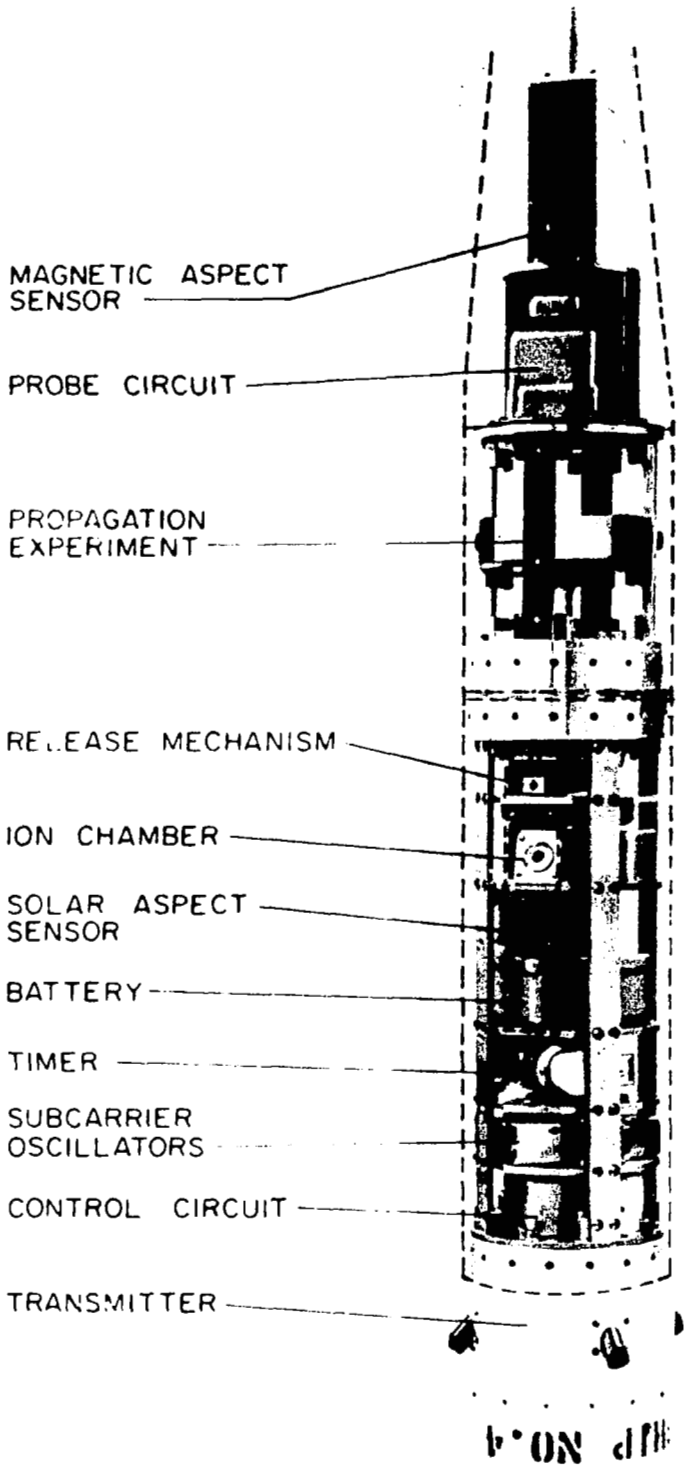

Figure 2. Payload Configuration.

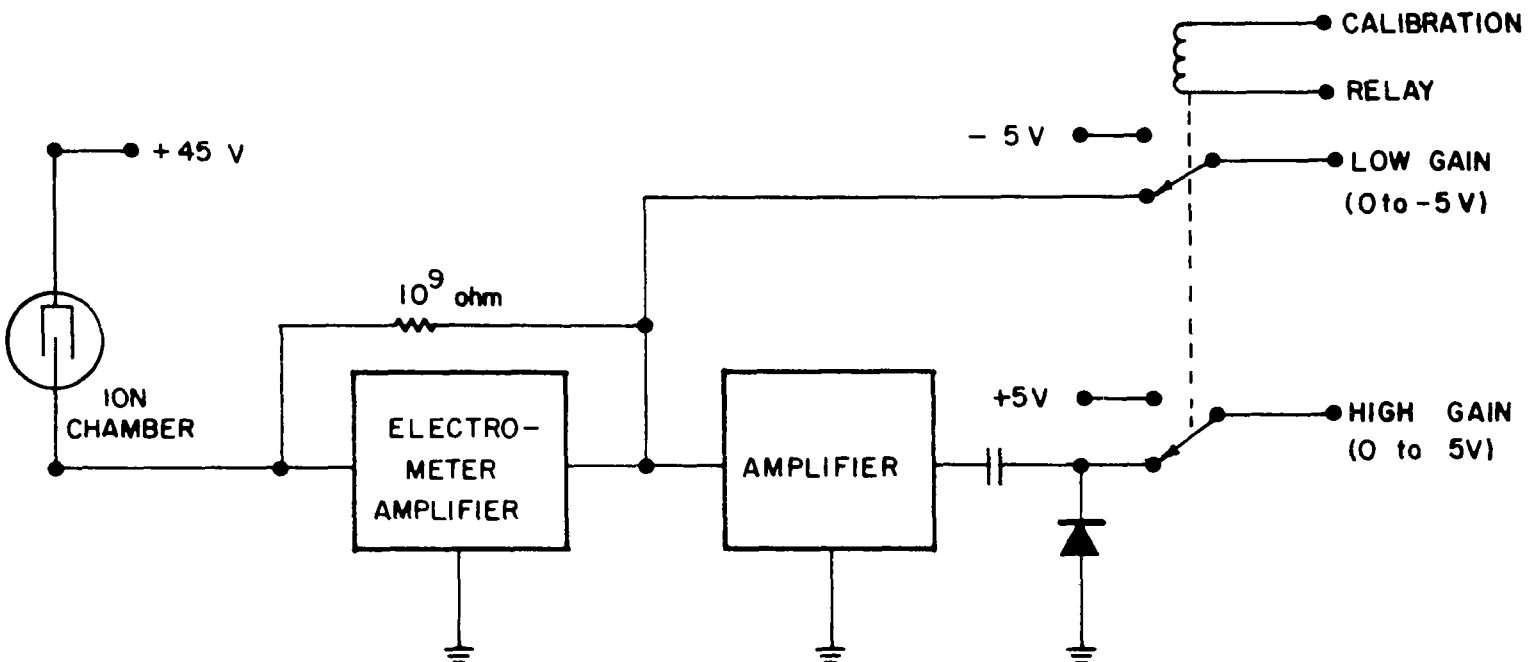

Figure 3. Block diagram of electronics.

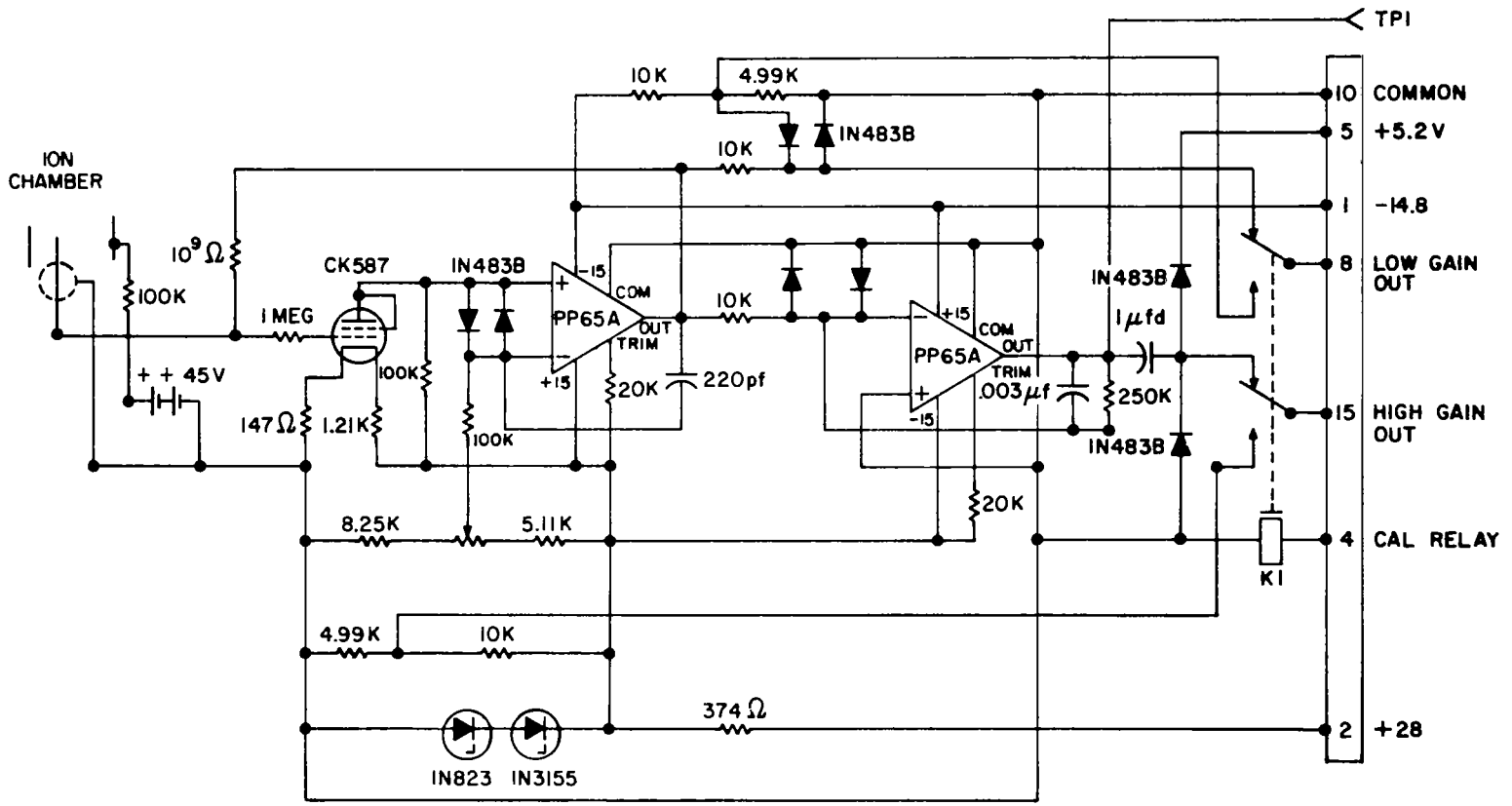

Figure 4. Schematic of electronics.

CHANNELS

The low-gain and high-gain ~~chambers~~ of the telemetry system are calibrated by applying 5 volts directly to the input of the respective SCO. The calibration is applied when the calibration relay is energized. In-flight calibration is effected by the timer.

The low-gain channel allows measurements of currents from 5×10^{-11} to 5×10^{-9} A, while the high-gain channel has a range of 2×10^{-12} to 2×10^{-10}, representing a dynamic range for the Lyman-α profile of $5 \times 10^{-9}/2 \times 10^{-12} = 2500$. This provides a favorable margin of safety against poor aspect conditions and low sensitivity.

LYMAN-α ION CHAMBER RESPONSE

The desired low wavelength cutoff for the ion chambers is achieved by the use of a lithium fluoride window. A 1 to 2 mm thick sample provides a transmission cutoff at 1050Å. Two different gas fills were used in the eclipse project, 15 mm of CS_2, and in the IQSY project, 20 mm NO. Although the 1240Å high wavelength ionization cutoff of the CS_2 provides a narrower bandpass than the 1350Å cutoff of NO, it was found in the eclipse project that the CS_2 became degraded during flight, altering the response of the ion chamber [4]. Consequently, in the later measurements, NO gas fill was used which with the lithium fluoride windows provided the bandpass 1050Å to 1350Å. The pronounced degragation observed with the CS_2 filled ion chambers was considerably reduced when NO was used.

The typical quantum yield (photoelectrons/quantum) for these two gases is given in Figures 5 [5] and 6 [6]. Not all ion chambers, however, have the actual response shown here, primarily because of differences in the transmission of the lithium fluoride windows. Differences in the quality of the crystal and contamination of the window surface, particularly the absorption of water vapor from the air causes these differences. These changes are not significant, however, except from the point of view of aspect corrections. Since the response is considerably greater at Lyman-α (1215.7Å) than near the high and low wavelength cutoffs, the effect of the radiation near the bandpass limits is small.

The incident intensity of Lyman-α is 3 to 6 ergs/cm^2 sec, and it dominates the radiation in the wavelength band 1050 to 1350Å. Various estimates indicate that it constitutes at least 80 to 90% of the total photon flux at the top of the atmosphere. By the time the Lyman-α reaches the vicinity of unit optical depth, the rest of the radiation in the bandpass has been strongly attenuated by the atmosphere. Only the very small amount of radiation at the wavelengths 1187, 1167, 1157, 1143 and 1108Å is absorbed by the atmosphere with comparable cross section (4×10^{-21} to 2×10^{-20} cm^2). Thus, by the time the measured flux has been reduced about 90% from the incident value, Lyman-α constitutes virtually 100% of the measured ion chamber response.

As is shown below (Analytical Expressions), absolute calibration of the ion chambers is not necessary for the determination of the molecular oxygen number density profile. However, for the eclipse project the necessary instrumentation was available so that the sensitivity (to Lyman-α radiation) of the ion chambers was determined by the technique outlined in Appendix A. Typical values range from 2×10^{-20} to 1×10^{-19} A sec cm^2/photon. For the IQSY study, the response of the ion chambers to an unknown but constant Lyman-α flux, compared with that of ion chambers serving as secondary standards, provided information as to the range of currents to be expected during flight. An almost pure Lyman-α flux in the range 1050 to 1350Å was obtained in the laboratory from a dc discharge in a low pressure mixture of four parts of helium to one part of hydrogen [7].

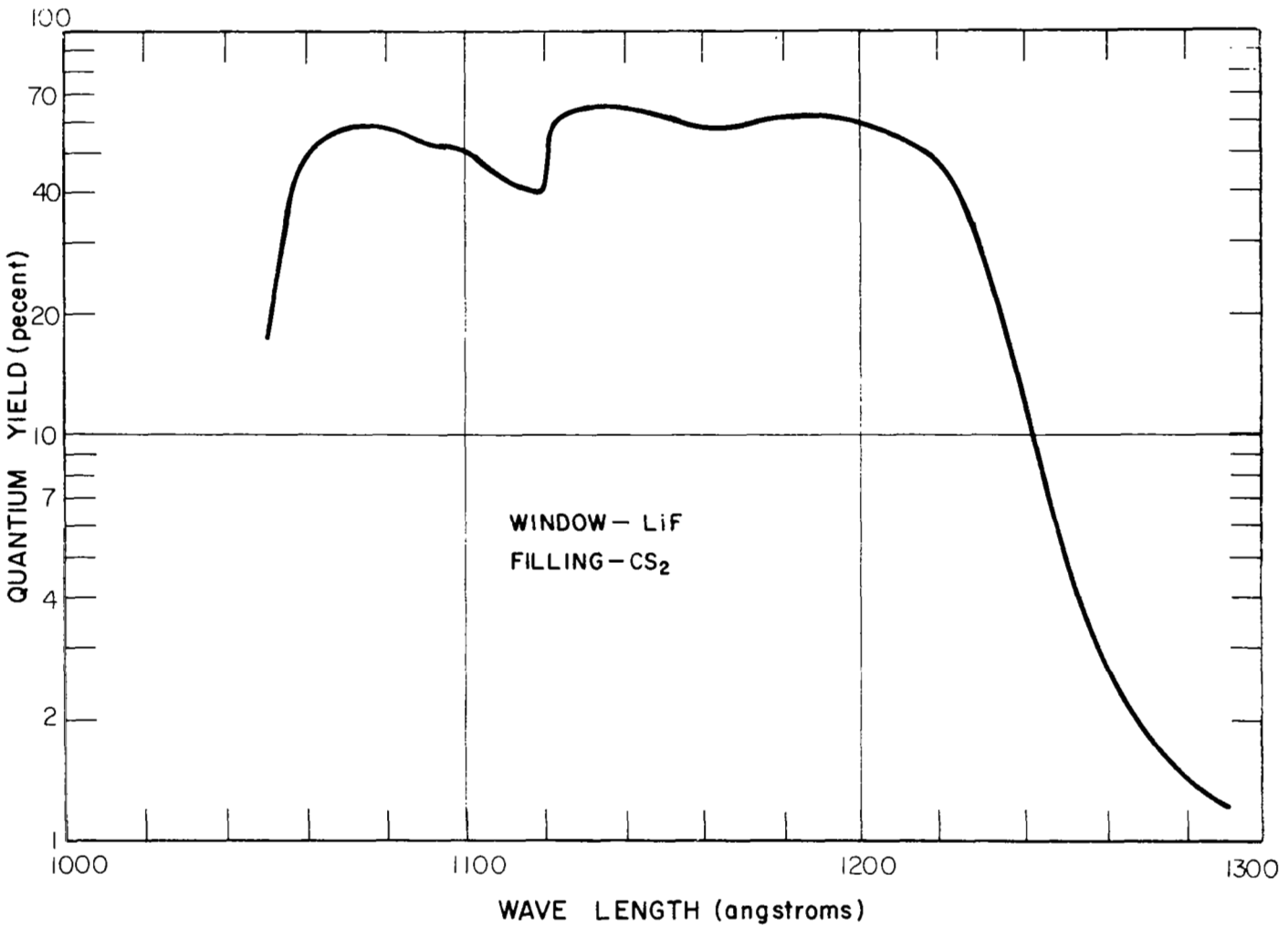

Figure 5. Spectral sensitivity of Lyman-alpha ion chamber (CS_2 gas fill).

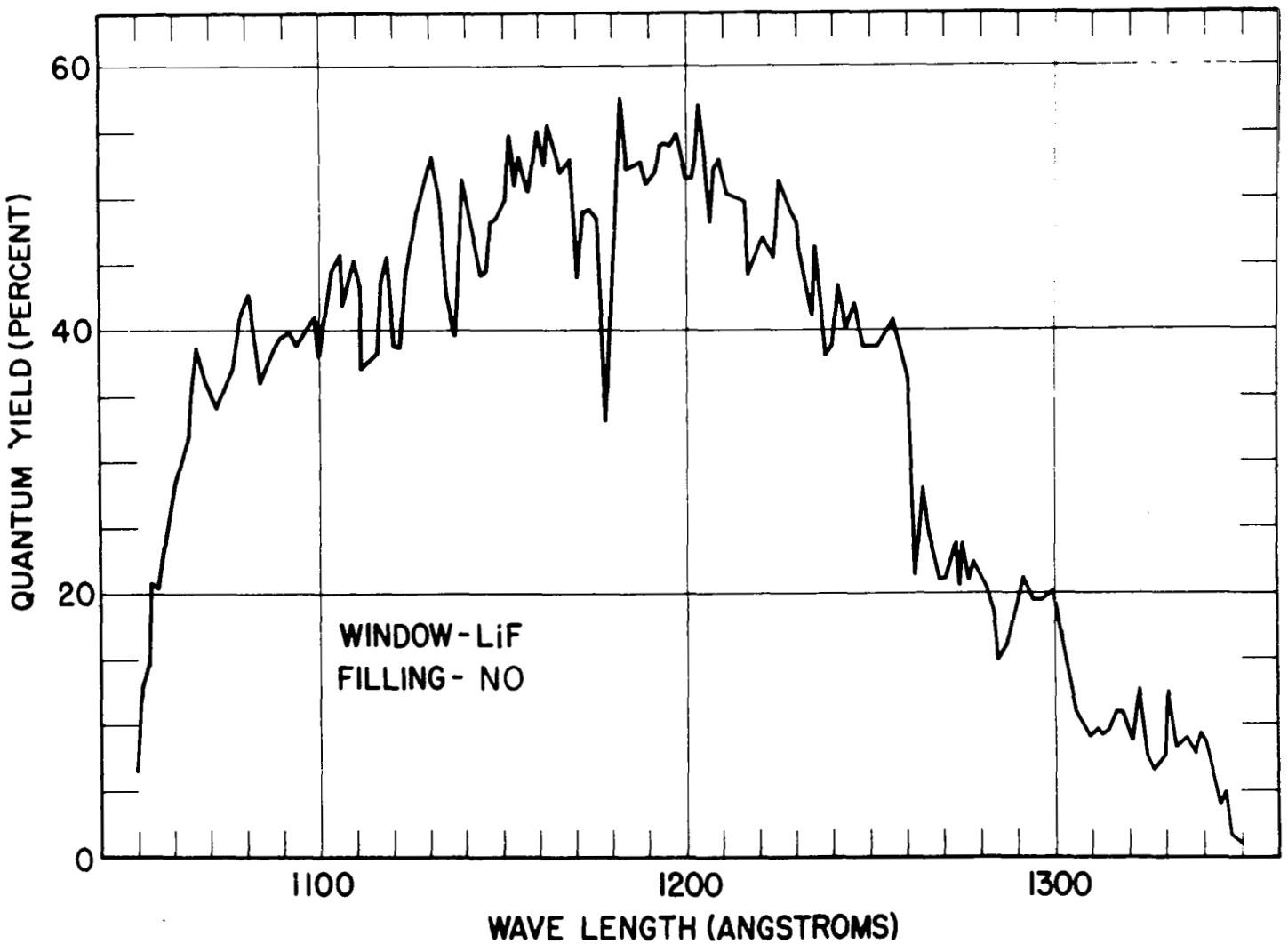

Figure 6. Spectral sensitivity of Lyman-alpha ion chamber (NO gas fill).

ASPECT SENSITIVITY OF ION CHAMBER

The response of the Lyman-α ion chambers is dependent on the direction of the incoming radiation. This change in response is due to several factors whose net effect is to reduce the efficiency of the ion chamber as the angle of incidence for the incoming radiation (aspect angle) is increased. Because the aspect situation continually changes during flight, the proper corrections to the measured ion chamber output current must be made so that all data may be referred to the same measuring conditions, conveniently taken to be normal incidence (zero aspect angle).

The efficiency of an ion chamber at normal incidence depends on the transmission of the window and the absorption of the gas fill for the incoming radiation. At other than normal incidence, the path of the radiation in the window is increased and the path in the gas may be increased or decreased depending on geometry. In addition, at non-normal incidence, there is a reduction in the incident radiation because of the smaller projected area of the window in the direction of the incoming flux. This reduction factor is cos α, where α is the aspect angle. Edges around the window may also reduce the flux, particularly at large aspect angles.

For the ion chamber design used in the present study, there is no reduction of the path of the radiation in the gas until the aspect angle is greater than about 23°. For an aspect angle of 30°, the path in gas is only reduced about 16%. This will reduce the percentage of flux (Lyman-α) absorbed in the gas only about 2%. Since aspect angles larger than 30° can be avoided by a suitable orientation of the chamber within the payload, any changes in efficiency due to a reduced radiation path in the gas are neglected here. Also the effect of edges on the amount of flux entering the ion chamber will be negligible for such aspect angles.

The change in window thickness for oblique incidence results in a reduction of transmission that depends on the fraction of radiation transmitted by the window at normal incidence T. If the radiation traverses the window at an aspect angle α, the fraction of radiation transmitted will be given by

$$T(\alpha) = \exp[\ln T \cdot (\sec\alpha - 1)]. \qquad (1)$$

However, since the index of refraction n of the window will be greater than unity, the path of radiation will be reduced somewhat. It is found that the fraction of radiation transmitted is then given by

$$T(\alpha,n) = \exp\left\{\ln T \cdot \left[\frac{n}{\sqrt{n^2 - \sin^2\alpha}} - 1\right]\right\} . \qquad (2)$$

Thus the total aspect correction to be applied to the measured ion chamber output current $I(\alpha)$ is given by:

$$I(0) = I(\alpha) \cdot \sec\alpha \exp\left\{\ln T\left[1 - \frac{n}{\sqrt{n^2 - \sin^2\alpha}}\right]\right\} . \qquad (3)$$

For lithium fluoride, the index of refraction in the ultraviolet has been measured [8], and a value of 1.608 for Lyman-α is used here. This allows the aspect correction to be computed in terms of the window transmission at normal incidence. The change in transmission for different lithium fluoride windows is probably due to different amounts of water vapor absorbed onto a small surface layer and will not alter the value of n. Figure 7 shows the computed change, normalized to $\cos\alpha$, for several typical window transmission values.

For a 20-mm filling of nitric oxide gas, 97.6% of the Lyman-α radiation transmitted by the window is stopped in the gas. The relation between window transmission and ion chamber sensitivity S in A sec/photon is therefore given by:

$$S = 1.26 \times 10^{-19} T, \qquad (4)$$

where the photoionization efficiency of the nitric oxide is taken to be 81%. From an absolute calibration of the ion chamber, it is then possible to determine the required aspect correction from the aspect angle data. Fortunately, the experiments can be usually designed so that the aspect angles encountered during flight, are less than 15°. It is seen from Figure 7 that to within 3% error, the simple $\sec\alpha$ correction can then be used.

The aspect sensitivity of the ion chamber can be determined experimentally during the calibration procedure. However, it is difficult to obtain the required accuracy in the laboratory. It is preferred to use an aspect calibration obtained during the flight by making use of the rocket precessional motion. Near rocket apogee the solar flux may be assumed constant and the variation in ion chamber current considered to be entirely caused by change in aspect angle. The ratio of the current at an aspect angle α to that at normal incidence ($\alpha = 0^{\circ}$) is plotted against angle to give the calibration curve.

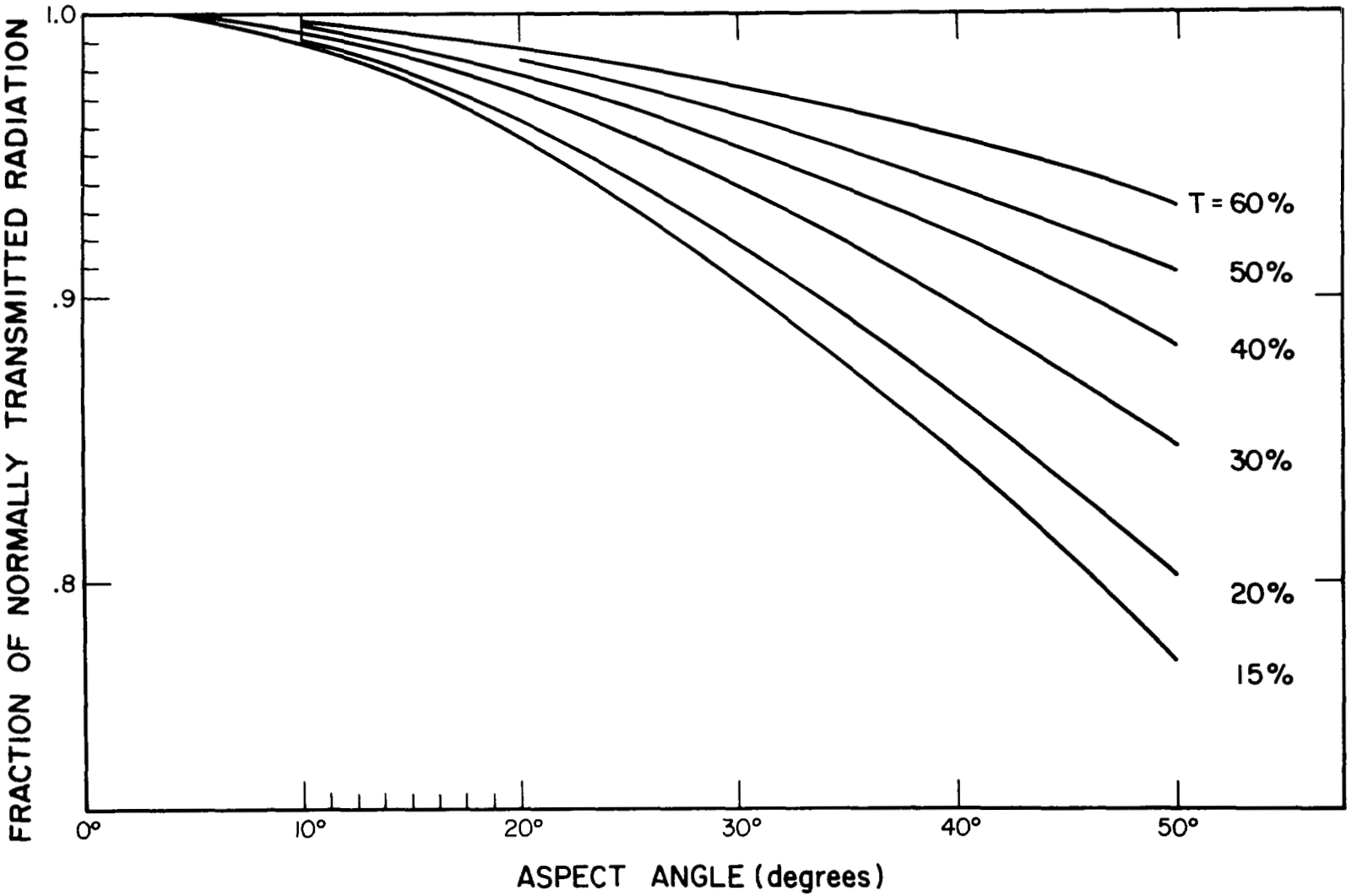

Figure 7. Reduction of ion chamber efficiency due to increased radiation path in window for typical values of T.

ANALYTICAL EXPRESSIONS

The flux of radiation at the observing point is related to the incident flux by the following expression:

$$I = I_o \exp(-\sigma n_T) \tag{5}$$

where σ is the absorption cross section at the wavelength of the radiation (assumed monochromatic) and n_T is the columnar number density between the source and the observing point. Since the assumption of a monochromatic response is valid for this ion chamber, the quantity I can also be considered to represent the measured ion chamber output current in the formulae that follow.

Equation (5) is generally used in its differential form:

$$\frac{1}{I}\frac{dI}{dz} = -\sigma \frac{dn_T}{dz} \tag{6}$$

The evaluation of n_T for the earth's atmosphere in the most general case presents considerable mathematical difficulty [9]. Fortunately several approximate expressions of sufficient accuracy for the present application have been developed.

When the solar zenith angle is not too large, the curvature of the earth may be ignored. Then from Figure 8a,

$$\frac{dn_T}{dz} = -n(z) \cdot \sec\chi \tag{7}$$

Thus, substituting in Equation (7) and re-arranging,

$$n(z) = \frac{1}{\sigma \sec\chi} \cdot \frac{1}{I}\frac{dI}{dz} \cdot \tag{8}$$

When used for determination of molecular oxygen in the upper atmosphere by absorption of Lyman-α, this formula, obtained in the flat-earth approximation, results in an error of no more than 1% for $\chi \leq 73^o$. The error is 10% at 85^o and increases rapidly for greater zenith angles. A formula

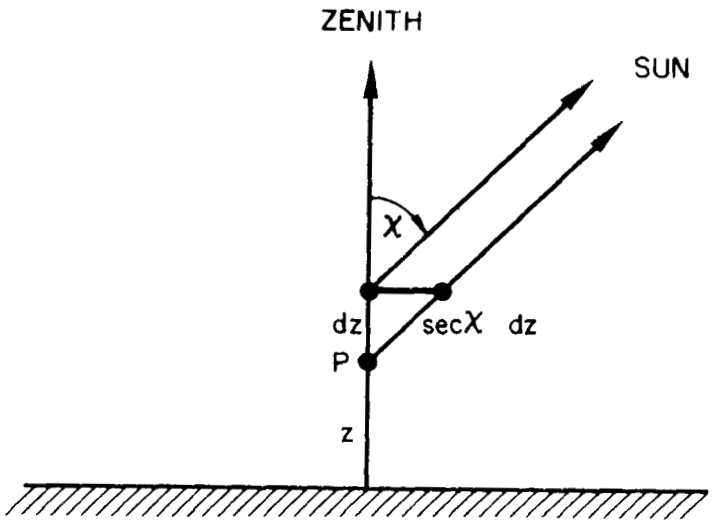

(a) FLAT EARTH APPROXIMATION

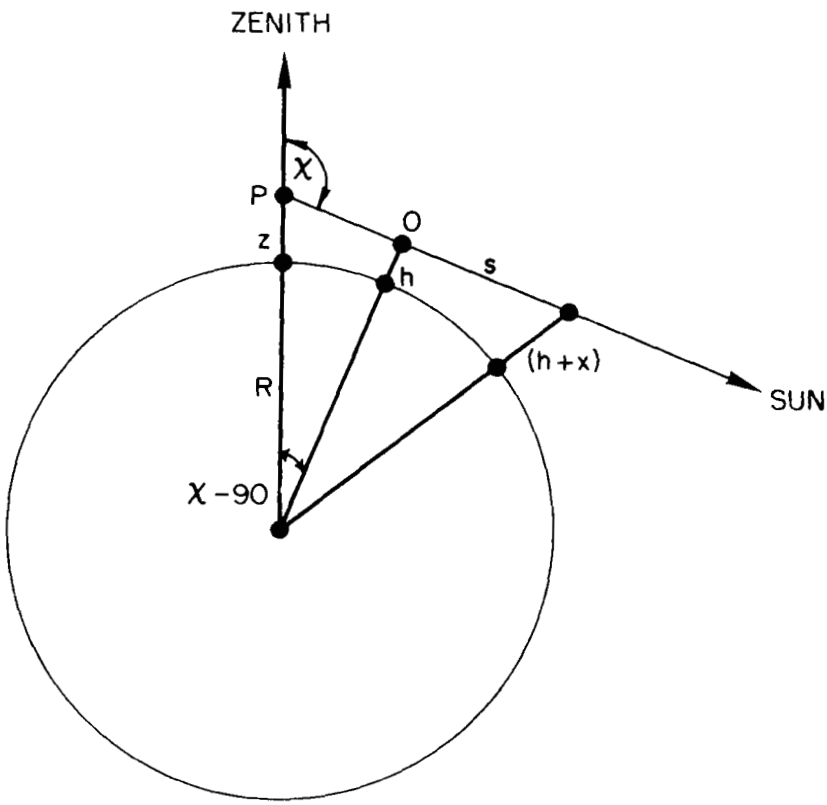

(b) GENERAL CASE $\chi > 90°$

Figure 8. Geometry for incoming radiation.

the range $85 < \chi \leq 90^{o}$ is adapted from the general case of $\chi > 90^{o}$.

The geometrical situation for $\chi > 90^{o}$ is shown in Figure 8b. The ray from the sun to the rocket at P passes the point of maximum particle density at point 0 above the earth's surface. It is assumed that the earth is spherical and that refraction is negligible. Since most absorption is taking place in the vicinity of the point 0, the intensity measured at P ultimately leads to the number density at 0. In this case it is therefore convenient to define the rocket position in terms of the minimum ray height which is given by

$$h = (R + z) \cos(\chi - 90) - R. \tag{9}$$

By integrating along the ray from the rocket to the sun, one obtains the columnar density $n_T(h)$. Measuring distance s along the ray from 0,

$$n_T(h) = \int_0^{\infty} n \, ds + \int_0^{P} n \, ds. \tag{10}$$

In order to evaluate the integrals it is necessary to specify the variation of n with height. Assume an exponential form defined by the scale height H. Thus,

$$n(x) = n(h) \cdot \exp(-x/H), \tag{11}$$

where n(x) is the number density at a height (h + x) above the earth's surface and n(h) the value at the height h. Using Equation (11) and the relation between s and x,

$$s^2 = (R + h + x)^2 - (R + h)^2 = x(2R + 2h + x), \tag{12}$$

it is easily shown that

$$\int n \, ds = n(h) \cdot \int \frac{(R + h + x) \exp(-x/H)}{x^{\frac{1}{2}} (2R + 2h + x)^{\frac{1}{2}}} \, dx \tag{13}$$

Since over the region of the importance in the calculation, R is much greater than h and x, this approximates to

$$\int n\, ds = n(h) \cdot \left(\frac{R}{2}\right)^{\frac{1}{2}} \cdot \int \frac{\exp(-x/H)}{x^{\frac{1}{2}}}\, dx \tag{14}$$

Setting $u^2 = x/H$,

$$\int_o^P n\, ds = n(h) \cdot (2RH)^{\frac{1}{2}} \cdot \int_o^{u'} \exp(-u^2)\, du = n(h) \cdot \left(\frac{\pi RH}{2}\right)^{\frac{1}{2}} \cdot \operatorname{erf} u' , \tag{15}$$

where $u = u'$ at the rocket position P. Noting that erf $u \approx 1$ for large u, it is found that

$$n_T(h) = n(h) \cdot \left(\frac{\pi RH}{2}\right)^{\frac{1}{2}} \cdot (1 + \operatorname{erf} u'), \tag{16}$$

where u' is given by

$$u' = \left(\frac{z-h}{H}\right)^{\frac{1}{2}} \approx \frac{(\chi - 90)}{H^{\frac{1}{2}}} \tag{17}$$

with χ in degrees and H in km. Thus u' is nearly independent of h and the factor $(1 + \operatorname{erf} u')$ may be regarded as constant when Equation (16) is differentiated with respect to h to obtain:

$$\frac{dn_T}{dh} = \left(\frac{\pi RH}{2}\right)^{\frac{1}{2}} \cdot (1 + \operatorname{erf} u') \cdot \frac{dn}{dh} \tag{18}$$

or

$$\frac{dn_T}{dh} = -n(h) \cdot \left(\frac{\pi R}{2H}\right)^{\frac{1}{2}} \cdot (1 + \operatorname{erf} u') \tag{19}$$

since

$$\frac{dn}{dh} = - \frac{n(h)}{H} \tag{20}$$

Thus, from Equation (6), written in terms of h the minimum ray height, instead of z

$$n(h) = \frac{1}{\sigma F} \cdot \frac{1}{I} \frac{dI}{dh} \tag{21}$$

where

$$F = \left(\frac{\pi R}{2H}\right)^{\frac{1}{2}} (1 + \text{erf } u'). \tag{22}$$

Substituting for u′ from Equation (17) and using the value for R, with X in degrees, and H in km gives the optical depth factor F:

$$F \approx \frac{101.4}{H^{\frac{1}{2}}} \left[1 + \text{erf } \frac{(X - 90)}{H^{\frac{1}{2}}}\right] \tag{23}$$

Swider has pointed out that this formula agrees with an exact calculation within 1% for $90 \leq X \leq 100^{o}$, R+z = 6550 ± 130 km, and H ≤ 130 km [9]. The function

$$\mathcal{F}(X,H) = \left[1 + \text{erf } \left(\frac{X-90}{H^{\frac{1}{2}}}\right)\right]$$

is plotted against

$$\left(\frac{X-90}{H^{\frac{1}{2}}}\right)$$

in Figure 9. When $X \geq 93^{o}$, the rocket is for practical purposes above the absorbing region for molecular oxygen, and an error of no greater than about 10% results from approximating the error function to unity.

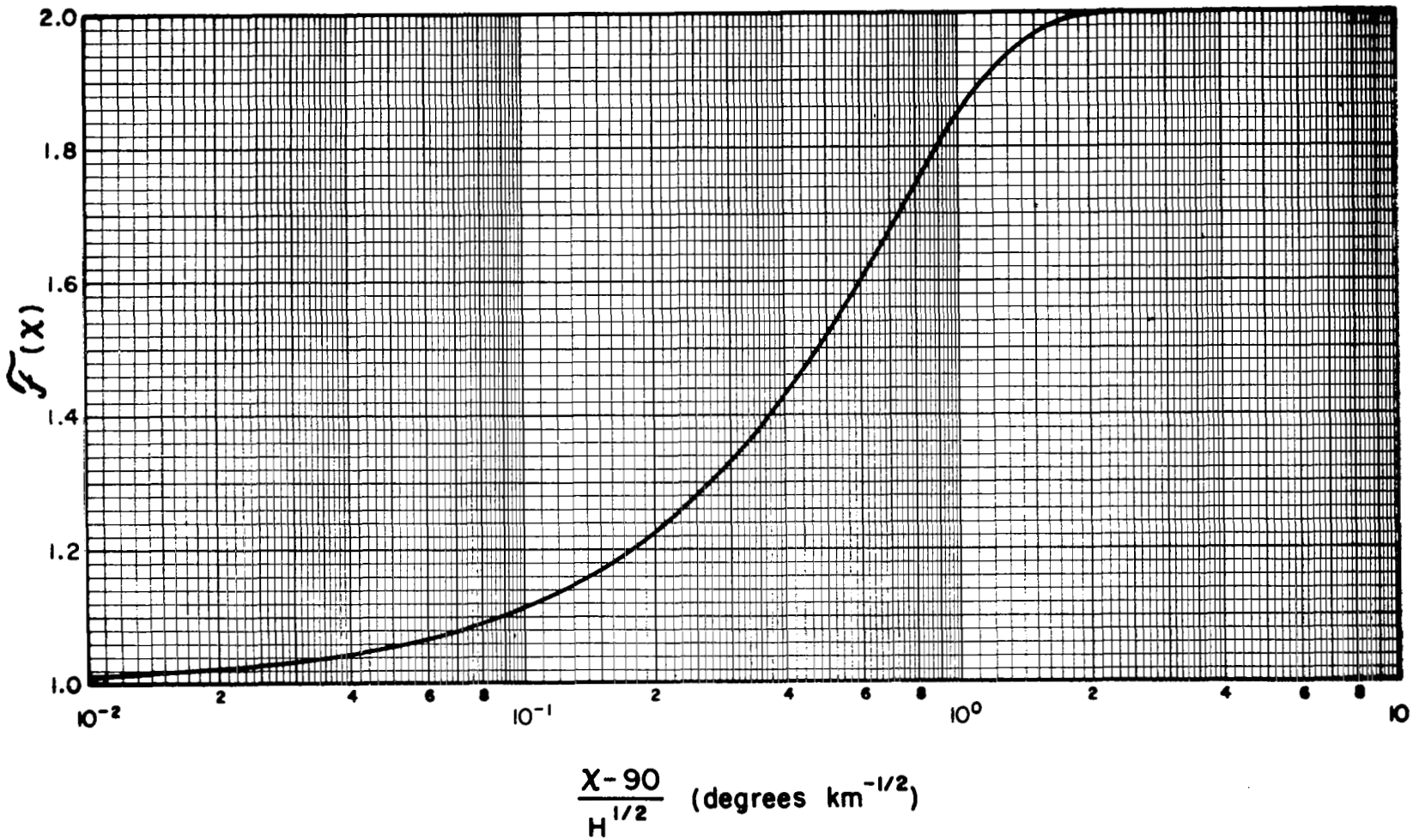

Figure 9. Variation of $\mathcal{F}$ for $X > 90^{o}$.

Then

$$F = \left(\frac{2\pi R}{H}\right)^{\frac{1}{2}} \approx \frac{202.8}{H^{\frac{1}{2}}} \qquad (24)$$

The error is no greater than 1% for $\chi \geq 100^{\circ}$.

The analysis given in Equations (9) through (23) can be utilized to obtain the function for $85 \leq \chi \leq 90^{\circ}$. In terms of what is now the virtual height h, Equation (16) becomes

$$n_T(h) = n(h) \cdot \left(\frac{\pi RH}{2}\right)^{\frac{1}{2}} \cdot (1 - \text{erf } u'). \qquad (25)$$

Transferring from the point of minimum ray height h to the rocket altitude z using

$$n(z) = n(h) \cdot \exp\left[-\frac{(z-h)}{H}\right] , \qquad (26)$$

Equations (21) and (23) are replaced by

$$n(z) = \frac{1}{\sigma F} \cdot \frac{1}{I} \frac{dI}{dz} \qquad (27)$$

and

$$F = \frac{101.4}{H^{\frac{1}{2}}} \cdot \left[1 - \text{erf } \frac{(90-\chi)}{H^{\frac{1}{2}}}\right] \cdot \exp\left[\frac{(90-\chi)^2}{H}\right] . \qquad (28)$$

The function

$$\mathcal{F}(\chi,H) = \left[1 - \text{erf}\left(\frac{90-\chi}{H^{\frac{1}{2}}}\right)\right] \cdot \exp\left[\frac{(90-\chi)^2}{H}\right]$$

is plotted against

$$\left(\frac{90-\chi}{H^{\frac{1}{2}}}\right)$$

in Figure 10. For zenith angles less than 85°, F may be approximated by sec X to an accuracy of about 10%.

The simplest formulae for the determination of concentrations by absorption spectroscopy with an error not exceeding about 10% are summarized in Table 1. The zenith angle limits corresponding to greater accuracy are given in Table 2. Formulae (21) and (27) show that it is not necessary to measure the incident flux or current at the top of the atmosphere in order to determine the oxygen concentration. Thus absolute calibration of the ion chamber is not required.

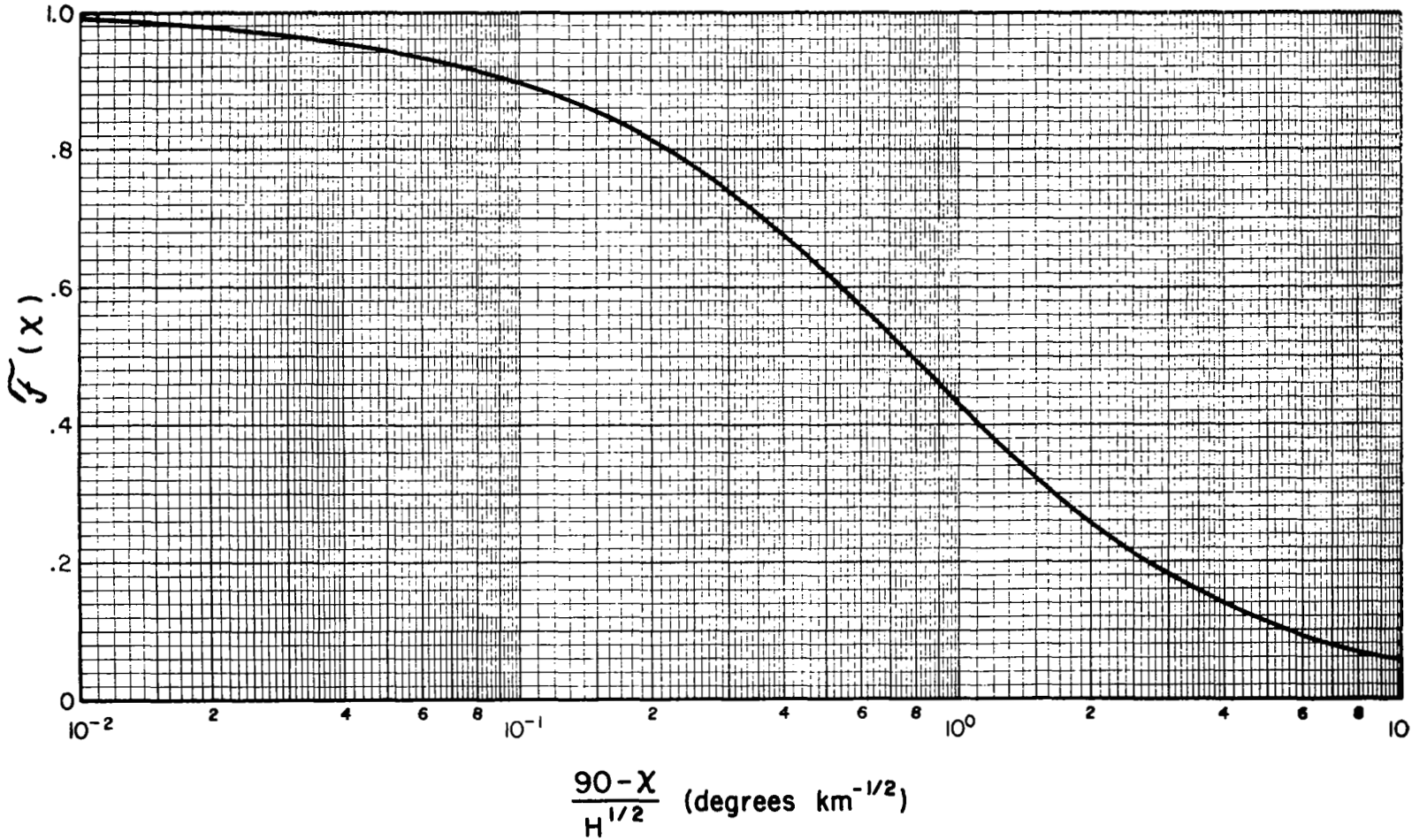

Figure 10. Variation in $\mathcal{F}$ for $\chi < 90^{\circ}$.

Table 1: Formulae for Computation of Particle Density by Absorption Spectroscopy with an Error not Exceeding about 10%.

(a) $\chi \leq 85^{o}$

$$n(z) = \frac{1}{\sigma \sec\chi} \cdot \frac{1}{I} \frac{dI}{dz} \tag{8}$$

(b) $85^{o} < \chi \leq 90^{o}$

$$n(z) = \frac{1}{\sigma F} \cdot \frac{1}{I} \frac{dI}{dz} \tag{27}$$

$$\text{where } F = \frac{101.4}{H^{\frac{1}{2}}} \cdot \left[1 - \text{erf}\left(\frac{90-\chi}{H^{\frac{1}{2}}}\right)\right] \cdot \exp\left[\frac{(90-\chi)^2}{H}\right] \tag{28}$$

(c) $90^{o} \leq \chi < 93^{o}$

$$n(h) = \frac{1}{\sigma F} \cdot \frac{1}{I} \frac{dI}{dh} \tag{21}$$

$$\text{where } F = \frac{101.4}{H^{\frac{1}{2}}} \cdot \left[1 + \text{erf}\left(\frac{\chi-90}{H^{\frac{1}{2}}}\right)\right] \tag{22}$$

(d) $93^{o} \leq \chi$

$$n(h) = \frac{1}{\sigma F} \cdot \frac{1}{I} \frac{dI}{dh} \tag{21}$$

$$\text{where } F = \frac{202.8}{H^{\frac{1}{2}}} \tag{24}$$

Note: (1) Measurements for $\chi > 90^{o}$ refer to point of minimum ray height.
(2) Units are: n cm^{-3}, σ cm^{2}, χ degrees, I arbitrary, z cm, h cm, H km.

Table 2a: Largest Zenith Angle for which the Approximation $F = \sec\chi$ is Valid for $H \approx 6.5$ km

Error	χ
10%	84.7°
5%	82.3°
2%	77.6°
1%	72.7°

Table 2b: Lowest Zenith Angle for which the Approximation $F = 202.8/\sqrt{H}$ is Valid

H (km)	$\chi_{10\%}$	$\chi_{5\%}$	$\chi_{2\%}$	$\chi_{1\%}$
7.5	93.17°	93.80°	94.50°	94.99°
7.0	93.06°	93.67°	94.35°	94.82°
6.5	92.95°	93.53°	94.19°	94.64°
6.0	92.85°	93.40°	94.03°	94.46°

COMPUTATION OF ZENITH ANGLE AND MINIMUM RAY HEIGHT

The solar zenith angle can be computed for any given point in the rocket trajectory from the radar data. The information which determines this angle is the latitude and longitude of the sub-rocket point (i.e., the point where the line from the rocket to the earth's center crosses the earth's surface) and the Universal Time. Data obtained from "The American Ephemeris and Nautical Almanac" (or its equivalent) of the appropriate year, is also required.

The formulae used in the zenith angle computation are:

$$h = \text{local sidereal time} - \alpha, \text{ and} \tag{29}$$

$$\cos \chi = \sin \varphi \sin \delta + \cos \varphi \cos \delta \cos h , \tag{30}$$

where h is the hour angle, α is the right ascention, φ is the latitude of sub-rocket point, and δ is the declination.

The minimum ray height, used when the zenith angle is greater than 90^{o}, can be obtained directly from the zenith angle (see Figure 11).

$$h = z \cos(\chi-90) - R[1-\cos(\chi-90)] \tag{31}$$

and the distance from the rocket to the point of minimum ray height from

$$s = (R+z) \sin(\chi-90). \tag{32}$$

Details of the computer program used to determine zenith angle and minimum ray height are given in Appendix B.

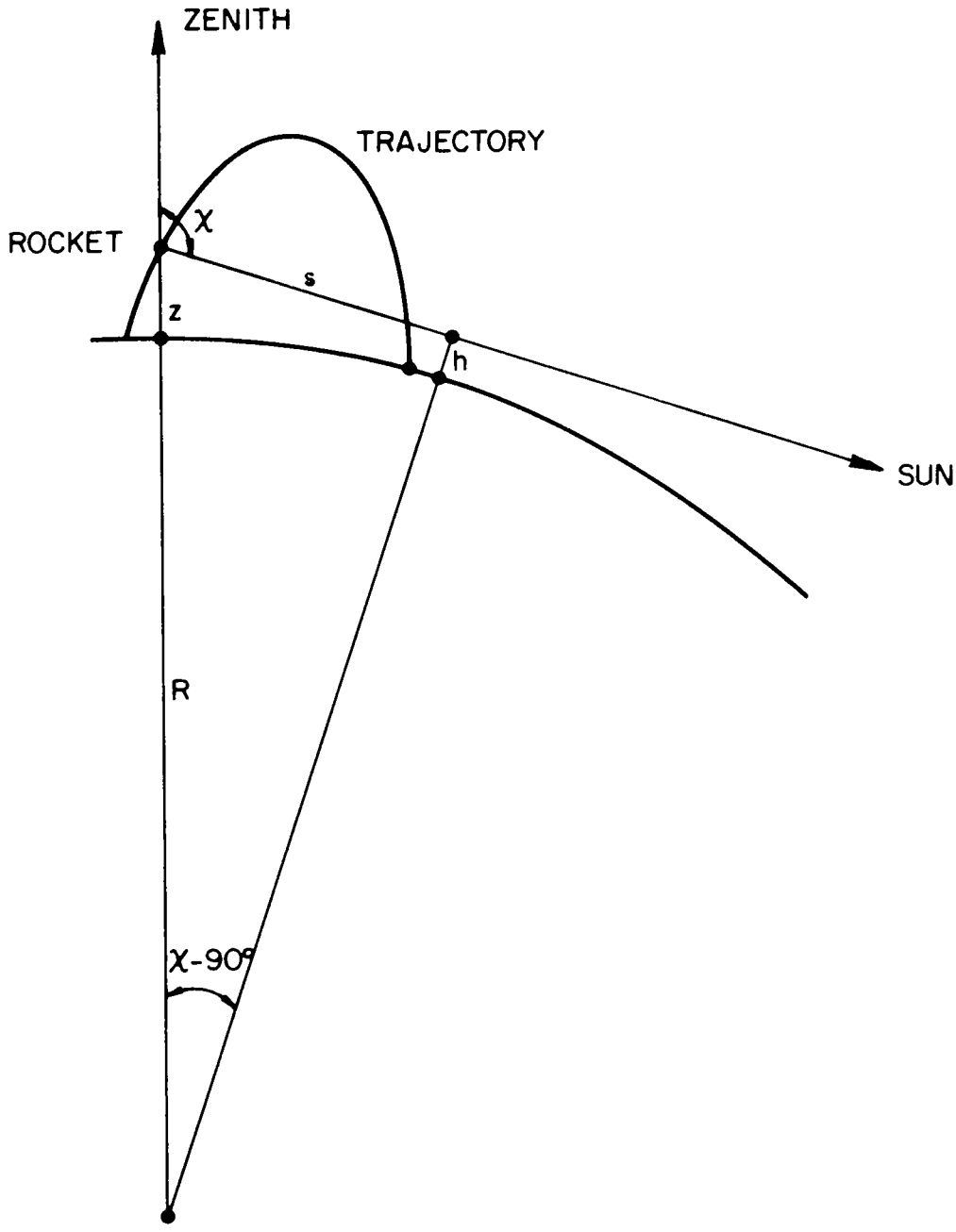

Figure 11. Minimum ray position and rocket trajectory for $\chi > 90^{o}$.

METHOD OF DATA ANALYSIS

Small Zenith Angles ($\chi \leq 90^{\circ}$)

(1) From telemetry record, using electrometer calibration and rocket trajectory data, obtain ion chamber current (I) as a function of rocket altitude (z).

(2) Using solar aspect sensor data, normalize current to a particular aspect angle (zero, if possible). This may be effected either from formula (3) (or Figure 7), which approximates $\sec\alpha$ for $\alpha \leq 15^{\circ}$, or from an equivalent empirical correction, obtained from the variation observed during constant flux conditions.

(3) Plot corrected ion chamber current versus z on a linear scale. From this plot obtain (1/I) dI/dh at given height intervals (1 or 2 km).

(4) Plot (1/I) dI/dz versus z and extract scale height H versus z.

(5) Determine optical depth factor $F(H,\chi)$ along the rocket trajectory, and compute $n[O_2]$ from formula (27):

$$n = \frac{1}{\sigma F} \frac{1}{I} \frac{dI}{dz} .$$

F is determined from $\sec\chi$ or formula (28), depending on the zenith angle and required accuracy.

Large Zenith Angles ($\chi \geq 90^{\circ}$)

(1) Same as for small zenith angles.

(2) Same as for small zenith angles.

(3) Using data derived from rocket trajectory, convert from rocket altitude z to minimum ray height h. Plot aspect corrected ion chamber current versus h on a linear scale. From this plot obtain (1/I) dI/dh at given height intervals.

(4) Plot (1/I) dI/dh versus h and extract scale height H versus h.

(5) Determine optical depth factor $F(H,\chi)$ versus h and compute $n[O_2]$ from formula (21):

$$n = \frac{1}{\sigma F} \frac{1}{I} \frac{dI}{dh} .$$

F is determined from formula (22) or (24), depending on the zenith angle and required accuracy.

ERROR DISCUSSION

Cross Section Errors

Reported values of the absorption coefficient of molecular oxygen at Lyman-α have ranged from .22 cm^{-1} to .28 cm^{-1} [10-14]. Thus systematic errors as large as 25% in the molecular oxygen number density may result from uncertainty in absorption coefficient. In this study Watanabe's value of .27 cm^{-1} (cross section of 1.00×10^{-20} cm^2) is used. When the density results of different investigators are compared, it is necessary to take into account cross section values that are used. Since the cross section uncertainty is systematic, it has no bearing on the determination of scale height.

Non-Ideal Behavior of Ion Chamber

The effect of radiation other than Lyman-α in the band pass of the ion chamber is to increase the value of n at high altitudes, i.e., in the region where the total incident radiation is reduced 10% or less. In the vicinity of unit optical depth, in a range of roughly 3 to 4 scale heights, depending on the zenith angle, it is estimated that the error from other radiation is no greater than a few percent at most.

At lower altitudes there may be errors resulting from other radiation that is absorbed less strongly than Lyman-α. At 1108.3 and 1187.1Å, the absorption coefficient for molecular oxygen are only .11 and .18 cm^{-1}, respectively. Since the solar radiation at these two windows is probably much less than 10^9 photons/cm^2/sec, the Lyman-α flux would have to be reduced more than two orders of magnitude before there would be any error introduced from this radiation. The effect would be to decrease the value of n from its true value.

Zenith Angle Errors

When the zenith angle is less than 85°, the uncertainty in number density due to an uncertainty in zenith angle is found from Equation (8) and is given by:

$$\delta n = n \tan \chi \, \delta\chi \, . \qquad (33)$$

From Equation (28), a more complicated relation is found for the case of $85^\circ \leq \chi \leq 90^\circ$. The results are plotted in Figure 12 for two typical values of $\delta\chi$.

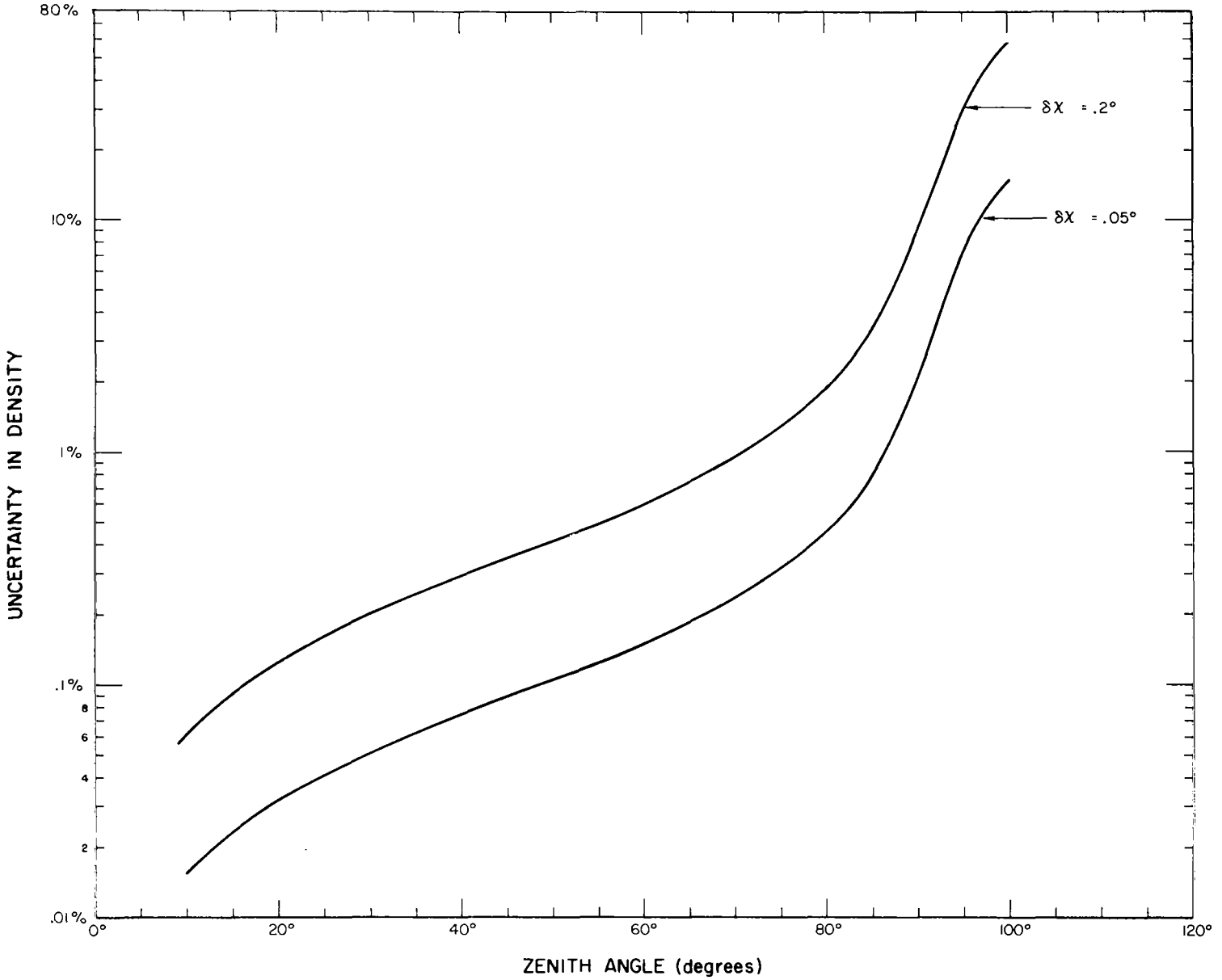

Figure 12. Uncertainty in density due to uncertainties in zenith angle.

When the zenith angle is greater than 90°, an uncertainty in χ causes an uncertainty in h as well as in F. Formula (31) is used to determine this height uncertainty according to

$$\delta h = R \sin(\chi - 90)\, \delta\chi \ . \qquad (34)$$

The uncertainty in number density due to this uncertainty in h is then given by:

$$\frac{\delta n}{n} = \frac{R}{H} \sin(\chi - 90)\, \delta\chi \ . \qquad (35)$$

Since the uncertainties in h and F are dependent, they are added to determine the total uncertainty in n due to an uncertainty in χ. These results are also plotted in Figure 12 for typical values of $\delta\chi$ and H = 6.5 km.

It is seen that much better accuracy is required in the zenith angle to make accurate density measurements at large zenith angles. As with cross section uncertainties zenith angle uncertainties will not affect the measurement of scale height.

Approximations in Mathematical Treatment

In the analysis for the case of $\chi > 90^{\circ}$ it has been assumed that the radius of the Earth is a constant equal to 6370 km. Since actual deviations from this value are no greater than .2%, 6370 km suffices for all calculations and introduces no significant error.

In formulae (22) and (25), the quantity (R+h) has been approximated by R. The numerical value of R that is used in the practical formulae (23), (24), and (28) is 6370 + 90 km and represents the best approximation of (R+h) over the range of h for which the technique may be used (60 to 120 km). Over this range of h the maximum error in $\sqrt{R}$ is then about $\frac{1}{4}$%.

In the determination of the optical depth factor F, it is assumed that the value of the scale height H is a constant. Further calculations have shown that the value of F is weakly dependent on the value of this gradient [8]. Thus, an iteration process can be used to determine the value of F if sufficiently large gradients, about 1 km/km, are encountered.

Other Absorbers

Other absorbers in the height range 70 to 112 km that may absorb Lyman-α radiation significantly include water vapor and ozone, as they have high absorption coefficients of 387 and 614 cm^{-1} [15,16], respectively. If present in significant concentrations, these constituents would cause an apparent increase in the molecular oxygen concentration. Unfortunately, in this altitude range there is little experimental data available on the concentrations of these constituents, especially of water vapor.

To produce comparable absorption, the concentration of water vapor would have to be at least 1/1400 the concentration of molecular oxygen. The only available quantitative information on water vapor is obtained from a theoretical analysis of Bates and Nicolet [17]. Mean concentrations of molecular oxygen obtained from the U.S. Standard Atmosphere, 1962 indicates that the error introduced from Nicolet's water vapor profile would be approximately 3.8% at 70 km, .59% at 80 km, and less at higher altitudes.

For ozone to produce comparable absorption, the required concentration would have to be at least 1/2270 the concentration of molecular oxygen. For the error calculations, theoretical profiles by Barth are used [18]. If his "sunset" ozone profile is compared with standard atmosphere values for molecular oxygen, the error is .60% at 70 km, .35% at 80 km, and less at higher altitudes.

These calculations show that errors due to Lyman-α absorption by water vapor and ozone are probably small. Experimental data on the water vapor concentration will allow more accurate estimates to be made of its influence.

OBSERVATIONS AND DISCUSSION

The bandpass of the Lyman-α ion chambers allows accurate Lyman-α flux measurements over a range of at least a hundredfold, beginning at a height where there is about a ten-percent reduction of the incident flux. These altitudes, which represent the range for obtaining the molecular oxygen data, depend on the solar zenith angle because of the change in the radiation path. For example, at $\chi = 0^{\circ}$, this range is about 68 to 89 km; at $\chi = 85^{\circ}$, the altitude is increased to 79 to 108 km; and at $\chi = 95^{\circ}$, to 89 to 112 km. The circumstances for the two series of rocket flights, which have provided data on the molecular oxygen density, are summarized in Table 3.

Ion chamber data at large zenith angles obtained from Nike Apache flights 14.145 and 14.146 are shown in Figure 13. In flight 14.145 the effect of the small difference in the zenith angles of about 1.2 degrees between the ascent and descent portion of the trajectory is seen to have a pronounced effect on the profiles. In flight 14.146 the small zenith angle change between ascent and descent results more in a profile shape change. The intersection of the ascent and descent curves is partly due to this and partly due to a sensitivity change of about eight percent taking place near the top of the rocket trajectory. Since this sensitivity change takes place near zero optical depth for Lyman-α, it does not alter the final number density results.

The payloads used in the eclipse project at Fort Churchill, Manitoba, Nike Apache 14.91, 14.92 and 14.94, each contained two ion chambers, which provided data during the recovery phase at 92 percent and 85 percent solar obscuration and last contact. Since one of the ion chambers in flight 14.94 showed a significantly different profile and exhibited a pronounced degradation compared to the others, the data from it were discarded as being unreliable [4]. Although the other five ion chambers showed some degradation above 95 km, the results below 90 km are considered reliable. The molecular oxygen profiles were in close agreement with each other and showed no systematic variation with respect to the phase of the solar eclipse. Since these five measurements were also made within one hour and seven minutes of each other, it was considered valid to average all the data together. These results and the standard deviation in the mean are plotted in Figure 14.

Figure 14 also shows the data from Nike Apache flights 14.86, 14.145, 14.146 and 14.148. The estimated random uncertainties in the smoothed curves are to within five percent, except for the first 4 km of data for all four flights and the last 4 km of data for flights 14.145/6/8, where the uncertainties are ten percent or more. For flights 14.145/6, the data points are represented by scale heights of 6.6 km. Estimated zenith angle uncertainties of 0.05° will introduce negligible systematic errors in all flights except 14.145 and 14.148, for which the calculated uncertainty from Figure 12 is 7.5 percent. Including this independent source of error for flights 14.145 and 14.148, it is found that the uncertainties are within 9 percent, from 94 to 108 km and about 13 percent or more from 90 to ~~90~~ 94 km and 108 to 112 km. Uncertainties from

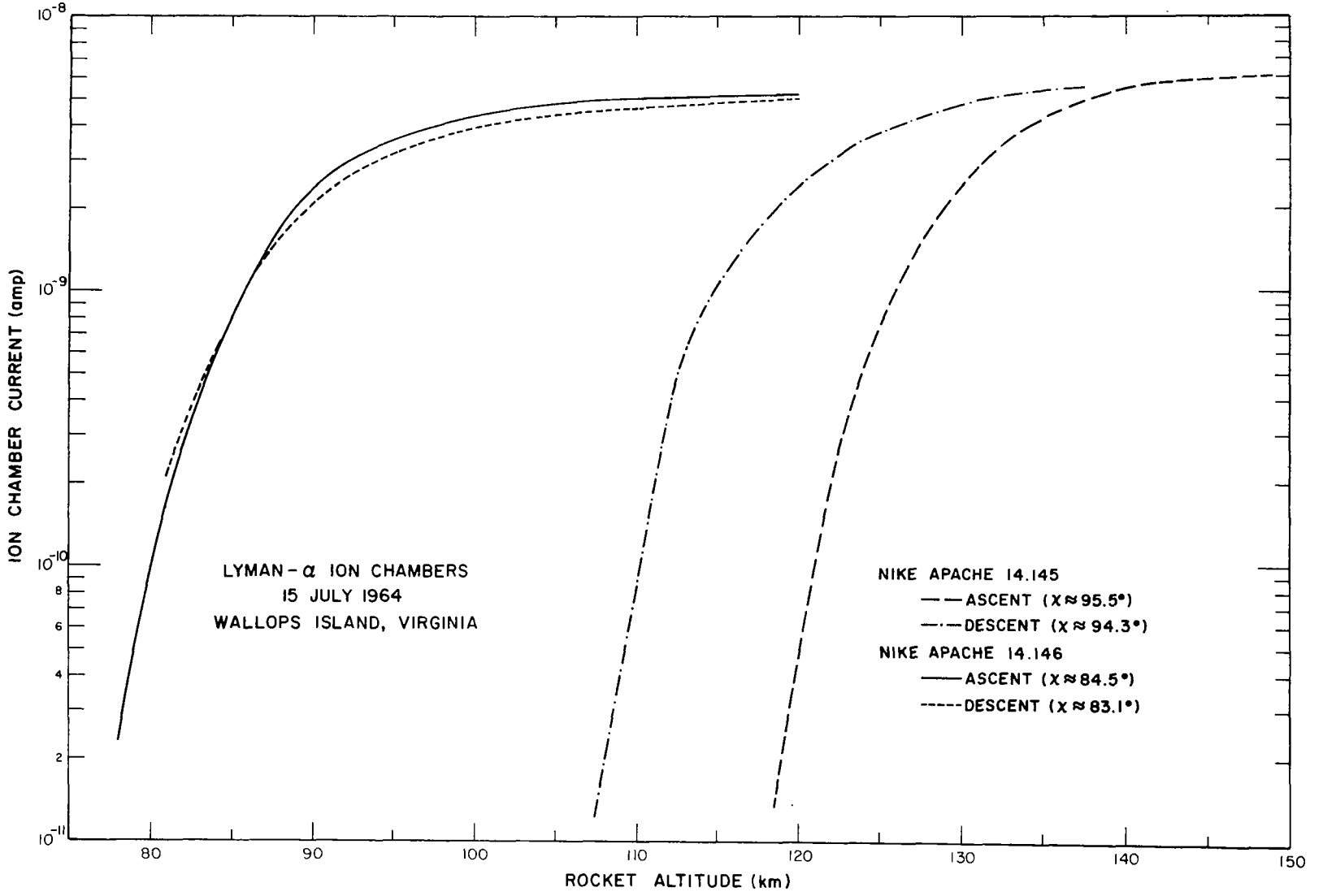

Figure 13. Typical ion chamber current profiles.

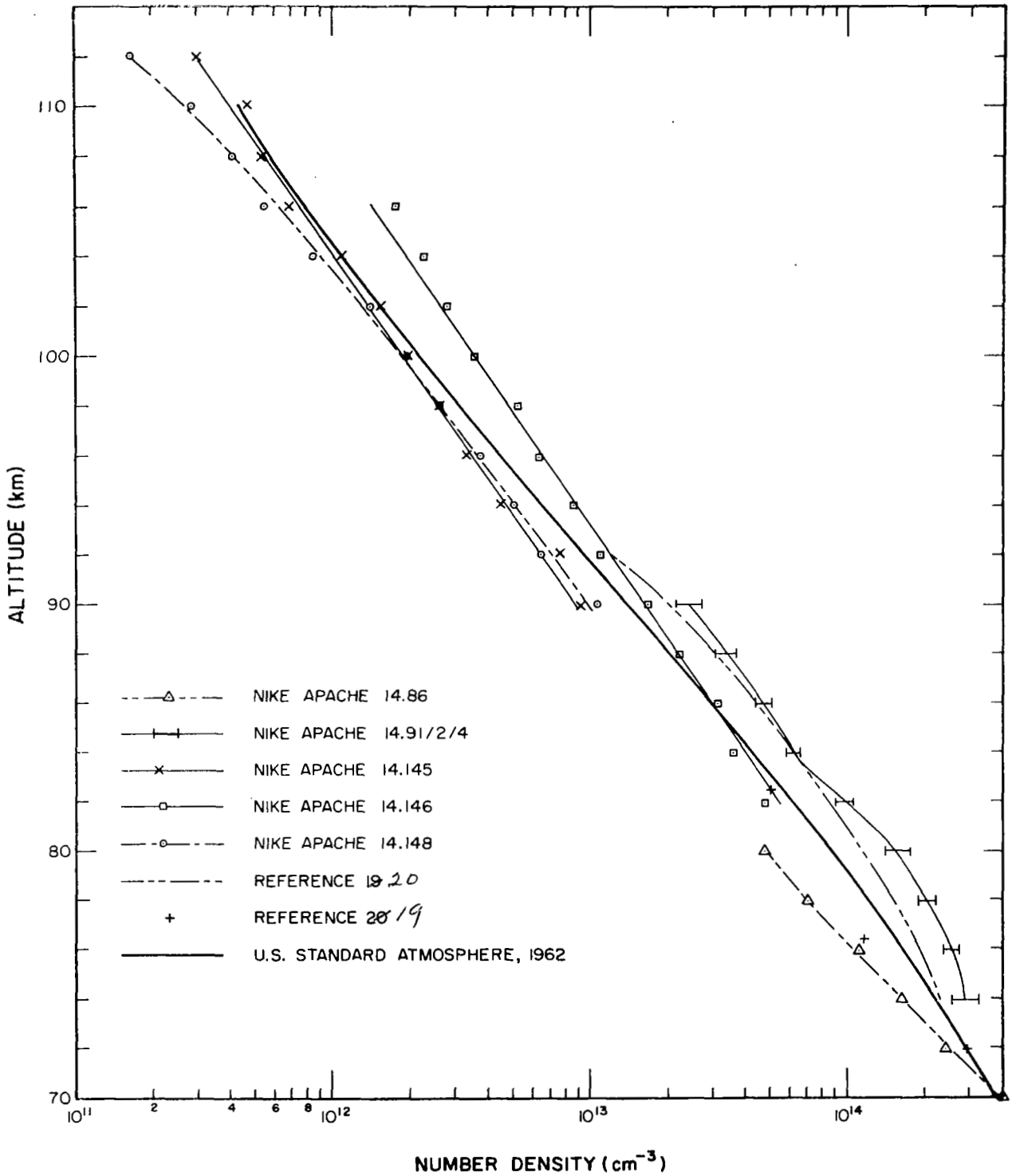

Figure 14. Molecular oxygen density profiles.

Table 3: Summary of Flight Circumstances

Nike Apache Designation	Date	Location	Ion Chamber Gas Fill	Solar Zenith Angle
14.86	27 Feb. 63	Wallops Island	CS_2	56^o
14.91	20 July 63	Fort Churchill	CS_2	48^o
14.92	20 July 63	Fort Churchill	CS_2	49^o
14.94	20 July 63	Fort Churchill	CS_2	56^o
14.145	15 July 64	Wallops Island	NO	95^o
14.146	15 July 64	Wallops Island	NO	84^o
14.148	19 Nov. 64	Wallops Island	NO	95^o

the absorption cross section or other absorbers have not been included in these estimates.

For comparison purposes, the molecular oxygen concentration as determined from the U. S. Standard Atmosphere, 1962 is also shown. This profile was obtained by taking 20.95 percent of the total number density and therefore does not include a reduction at higher altitudes resulting from a dissociation of molecular oxygen. This model is found to represent all the experimental data to within a factor of 2.3.

A significant increase in density is observed in the summer at Fort Churchill (Nike Apache 14.91/2/4) compared with Wallops Island data for summer (Nike Apache 14.145/6) and fall and winter (Nike Apache 14.86, 14.148). This is evidence of a high latitude increase in molecular oxygen concentration, at least during summer, for the altitude range 82 to 90 km.

The general agreement between flights 14.145 and 14.148 up to about 104 km both measured at a zenith angle of 95°, in contrast to 14.146 measured at a zenith angle of 84°, suggest that either there may be significant zenith angle effects or possibly a systematic error in the method of analysis when the zenith angle is larger than 90°. Additional measurements at Wallops Island for $X = 88$ to 90° should indicate whether this is a zenith angle effect. From about 104 km to 112 km, the summer values (flight 14.145) are greater up to a factor of 1.8. Further measurements at slightly higher altitudes will show if this is a seasonal effect.

For purposes of comparison, the results of other investigators using the method of Lyman-α absorption are shown in Figure 14. Carver, et al. [19], also used a Lyman-α cross section of 1×10^{-20} cm^2, but it was necessary to modify the data of Kupperian, et al. [20], by 28.5 percent in order to normalize it to this cross section. Also because Kupperian's measurements were extended to higher altitudes by observations of other spectral lines, the modified data are only plotted up to 92 km. The general agreement between Kupperian's summer measurements of 1957 with our measurements of 1964 suggests that there are no large solar cycle variations in molecular oxygen density at these altitudes. Kupperian's data practically lies within our error bars from 82 to 90 km. The deviations from our data are no greater than 26 percent over the entire range 74 to 90 km, and are less than 13 percent from 82 to 88 km. The approximate agreement of Carver's data from Australia in winter with our Wallops Island data of summer and winter, Nike Apache 14.86 and 14.146 supports our mid-latitude observations.

Data obtained by Jursa, et al. [21], from measurements at White Sands of the Schumann-Runge region by spectrographs during sunrise and sunset in March and October agree approximately with our mid-latitude data from 62 to 87 km. Above 110 km additional absorption spectroscopy data were obtained by Byram, et al. [22,23], using Geiger counters, sensitive to a band about 1450Å and

Hinteregger [24] using a spectrograph to measure 1206.5Å radiation. However, the investigations of Byram, et al., Kupperian, et al., and Hinteregger show substantial differences and suggest the need for further measurements at these altitudes.

CONCLUSIONS

The measurement of molecular oxygen concentration in the D and lower E regions using the absorption profile of Lyman-α determined by a rocket borne ion chamber is probably the simplest method for obtaining the profile of any constituent of the upper atmosphere and is as accurate as any other technique. The relatively large flux of Lyman-α in the solar spectrum and the coincidence of a small absorption cross section of molecular oxygen at this wavelength combine to produce a virtually monochromatic situation which is ideal for absorption spectroscopy.

The useful altitude range of the measurements depends on zenith angle: at $\chi = 0^{\circ}$ the range is about 68 to 89 km while for $\chi = 95^{\circ}$ the range is about 89 to 112 km. The greatest accuracy of measurement occurs at unit optical depth, where the rate of change of flux with height is a maximum. This altitude increases from 75 km, at $\chi = 0^{\circ}$, to 100 km, for $\chi \geq 93^{\circ}$.

A given error in the zenith angle causes the uncertainty in the density to increase significantly as the zenith angle increases. If zenith angle data of the required accuracy are not available, the measurements should be restricted to sufficiently small zenith angles. It is also desirable that the detector be oriented within the payload so as to keep the aspect correction small and hence minimize errors from this source.

Measurements at small zenith angles have the disadvantage that, below 100 km, as the rocket turns over on descent, large aspect corrections must be applied to the data. If it is desired that accurate descent data be obtained, zenith angles greater than about 94°, measured to high accuracy, are required. When other types of detectors are used with this technique to measure constituents at higher altitudes, this consideration does not arise as the important part of the profile is already obtained before the rocket begins to tip over.

One of the largest uncertainties in the measurements arises from the uncertainty in the absolute value of the cross section for absorption of Lyman-α radiation by molecular oxygen. Since this uncertainty is systematic, it has no bearing on conclusions that may be drawn concerning density variations at different times and places, provided these are normalized to the same cross section. A value of 1×10^{-20} cm^2 has been used in the present study. Neglecting this source of error, under ideal conditions of measurement, i.e., small aspect angle corrections and moderate zenith angles, at altitudes near unit optical depth, the accuracy is limited essentially only by the reading errors and trajectory errors, whose net effect might be kept to 1 or 2%. In practice the error is about 5% within one scale height of unit optical depth, increasing to about 10% near the limits of the useful altitude range. For large zenith and aspect angles the errors will be somewhat larger.

In the first series of rocket flights carbon disulphide was found to produce an apparent change in sensitivity when the ion chamber was first exposed to the largely unattenuated solar flux. In the subsequent series of flights, NO was used with satisfactory performance of the detectors and is therefore considered the preferred gas.

Absolute calibration of the ion chamber requires elaborate experimental techniques, but once one ion chamber has been calibrated, others can be calibrated relative to the standard with rather simple equipment. Exposure to a suitable UV source in a vacuum permits their response to be determined relative to the standard.

The Lyman-α absorption profiles obtained with ion chambers flown from Wallops Island, Virginia, and Fort Churchill, Manitoba, during various seasons and times of day, lead to the following observations concerning the molecular oxygen density:

(1) Data obtained in the altitude range 76 to 90 km at Fort Churchill showed no systematic change in density during the recovery phase of the partial solar eclipse of 20 July 1963 (92% maximum obscuration).

(2) Comparison of this eclipse data [(1)] with Wallops Island data indicates that in the altitude range 82 to 90 km the density in summer is 40 to 100% greater at high latitudes than at mid-latitudes.

(3) Data from two flights at $\chi = 95^{o}$ at Wallops Island, in summer and late fall, show agreement from 90 to 104 km. There is therefore no evidence for a mid-latitude seasonal variation in this altitude range. At higher altitudes the density in summer is larger than in the late fall with a maximum factor of 1.8 at 112 km.

(4) There is an apparent decrease in the density of 46% for observations at Wallops Island at $\chi = 95^{o}$ compared with those at $\chi = 85^{o}$ in the altitude range 90 to 102 km.

(5) The data at Fort Churchill obtained by Kupperian, et al. [20], in the summer of 1957 agrees with our data obtained during July 1963 [(1)] when adjusted to the same cross section. Comparison shows that any decrease in density at high latitudes at solar maximum relative to solar minimum is less than 13% from 82 to 88 km and is no greater than 26% from 74 to 90 km.

Verification of these results and further clarification will result from additional measurements at mid-latitudes in summer and high latitudes in winter. Evidence of density changes during sunrise and sunset should be examined in future rocket flights. No low latitude observations have been reported, but such observations would be valuable in the light of evidence of the latitude dependence.

APPENDIX A

ABSOLUTE CALIBRATION OF LYMAN-α ION CHAMBERS

The method used to calibrate the ion chambers is to measure the total photon flux emerging from the exit slit of the monochromator by means of a standard ionization chamber filled with nitric oxide gas and using the known photoionization yields of NO at Lyman-α (.81 ion-pair/photon) to determine the radiant flux. This flux is then compared to the output current of the ion chamber and a photoionization yield is obtained.

The standard ionization chamber and ion chamber to be calibrated are shown schematically in Figure A1. The standard ion chamber is 17.5 inches long with a one-inch spacing between two-inch-wide stainless steel collector plates. The collector plates are mounted on teflon plugs and connected to the voltage supply and micro-micro ammeter through kovar seals. The entire housing of the ion chamber is stainless steel. The entrance slit of the ion chamber, with its lithium fluoride window, is mounted on a kovar-glass seal which protrudes past the end of the parallel plate electrodes. This ensures that all the ions created are collected. Since the slit is sufficiently narrow, the cross section of the beam at the ion chamber is less than its window area. The ion chamber is mounted at the end of the standard ion chamber through an O-ring seal. The standard (ion chamber) is filled with nitric oxide to a pressure of from 3 to 4 mm Hg. The voltage between the plates is around 50V, on the plateau region of the ion current versus voltage curve.

The calibration procedure is as follows: entrance and exit slit widths on the monochromator are adjusted to give a 3Å wide band pass. This resolution is deemed suitable since there are no large and sudden changes in the absorption cross section of NO in the wavelength range 1050-1350Å. The standard is pumped down to a pressure of 10^{-5} mm Hg, then the output of the ion chamber is recorded over the range 1050 to 1350Å. Following this, the standard is filled with NO gas to 3 mm Hg as recorded on an oil manometer. The output current of the standard ion chamber is recorded as a function of wavelength. Finally, the NO is pumped out of the standard until a high vacuum exists again; then a second scan is taken with the ion chamber to establish the constancy of the light source during the calibration procedure.

From the definition of the photoionization yield, Y, we get

$$Y = \frac{\text{ions formed}}{\text{photons absorbed}} = \frac{I\ (\text{amps})}{e} \cdot \frac{1}{P},$$

where I(amps) is the current from the ion chamber in amperes, e the electronic charge, and P is the number of photons/sec which are absorbed. Under the present conditions of total absorption in the standard, P is also the absolute intensity entering the ion chamber. Thus, knowing Y for NO, we

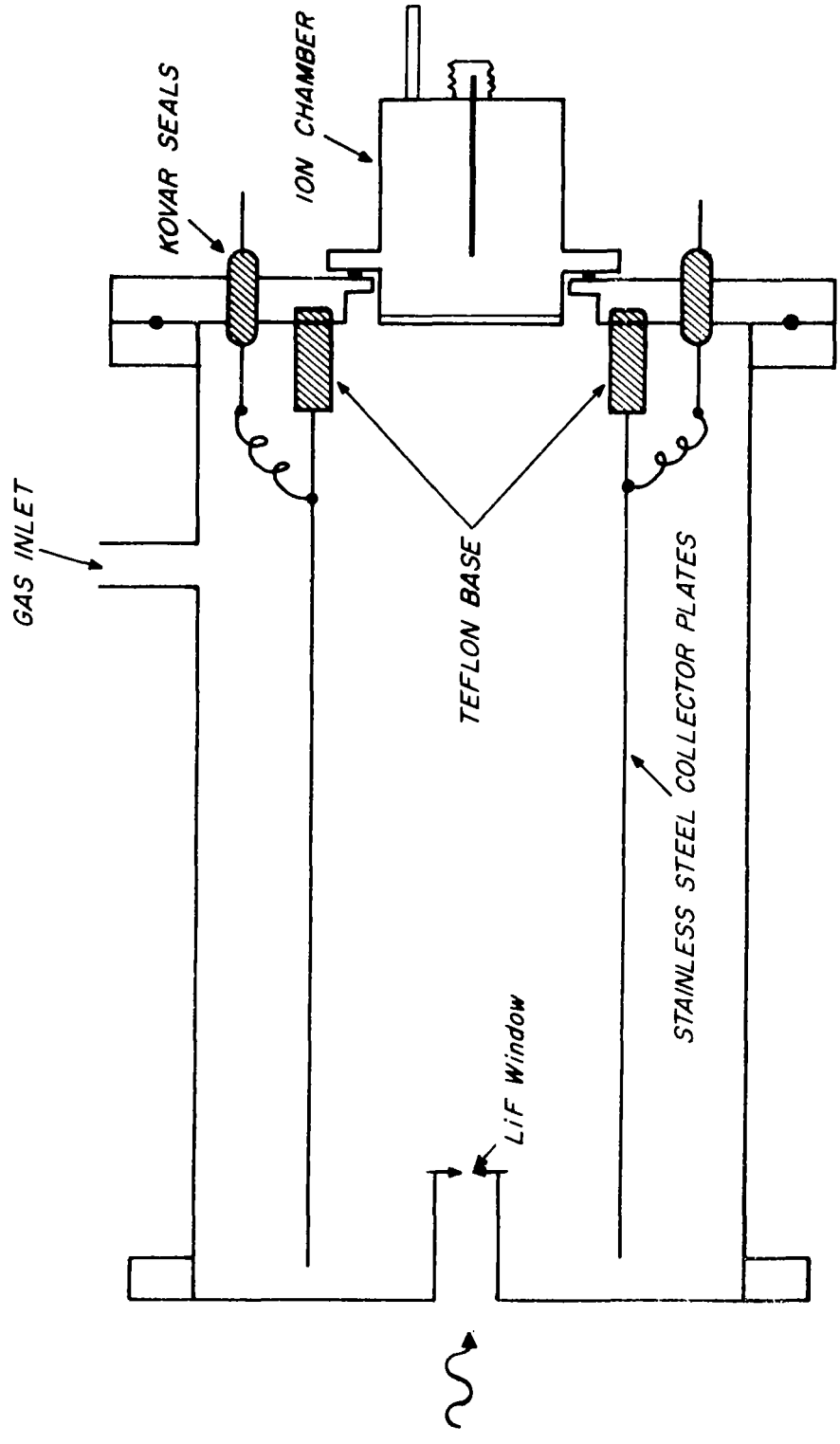

Figure A-1. Ion chamber calibration configuration.

can determine the absolute intensity, P, impinging on the window of the ion chamber as follows:

$$P = \frac{I\ (\text{amps})/e}{Y} \quad .$$

The ion chamber can thus be calibrated in terms of its output current per photon incident on its window/sec. If i(amps) is the current of the ion chamber and Y′ the photoionization yield of the ion chamber (this includes the attenuation of the LiF window), then

$$eY' = i(\text{amps})/P$$

and

$$Y' = Y\ i/I \quad .$$

The sensitivity is then given by

$$S = Y'/e.$$

APPENDIX B

COMPUTER PROGRAM IN FORTRAN LANGUAGE

A computer program in FORTRAN language is presented for the calculation of the zenith and azimuth angles of the sun from a rocket and the minimum ray height. This program is useful for making these calculations for any object of known ephemerides from any position on or near the earth.

In order to determine the correspondence between the labels on Figure 11 and the FORTRAN symbols, the following chart is provided.

Figure 11	FORTRAN Symbol
χ	ZEN
R	R
z	H, ALT
h	HGHT
s	DIST

The input is entered in card form in the order shown below:

Number of cards	Parameters
1	N1, N2, N3
N2	output heading cards
1	SIDM, PAR
1	RA, DRA1, DRAO
1	DE, DDE1, DDEO
N1	GMT, FLAT, FLONG, H

See the glossary at the end of Appendix B for the meanings of the parameters and the program listing for the format of the cards. The units of the parameters are: hours — SIDM, RA, GMT, FLONG; degrees — DE, FLAT; seconds — PAR, DRA1, DRAO, DDE1, DDEO; kilometers — H.

Most of the time it will be desirable to have the computer calculate the exact values of right ascention and declination. This is done in statements 15+1 and 15+2. These equations represent Stirling's interpolation formula to second order [where TT = u, DRA1 = Δy_{-1}, DRAO = Δy_0, RA = y_0, etc.] with appropriate conversion factors.* The terms DRA1, DRAO, DDE1, and DDEO are to be omitted if the exact values of the right ascen. ion and declination are to be entered.

*Notation taken from Numerical Mathematical Analysis, by J.B. Scarborough, Fourth Edition, The John Hopkins Press, Baltimore, Maryland, p. 74, 1958.

With the input to the zenith and azimuth equations available, the hour angle is calculated. The angles are converted to radians for computer use. An adjustment for parallax is available if desired.

The zenith and azimuth angles are now computed using standard formulas. These formulas involve no approximations and therefore are good to seven digits, corresponding to at least 0.036 seconds of arc. Therefore the accuracy of the zenith and azimuth angles is essentially limited only by the accuracy of the input data.

If the zenith angle is greater than 90^{o}, the shadow height is calculated. The radius of the earth needed for this calculation is obtained by using Hayford's spheroid as a model of the earth. The quantities HGHT and DIST are not meaningful unless the observer is above the surface of the earth, so if the zenith angle is greater than 90^{o} and $H \neq 0$, these quantities are calculated. The term H-HO is calculated only when HGHT is also calculated and $N3 \neq 0$.

The output is in the form of punched cards in the order shown below:

(Heading Cards)
GMT
LAT
LONG
ALT
ZEN
AZIM
SHDW (if ZEN $> 90^{o}$)
HGHT (if ZEN $> 90^{o}$, $H \neq 0$)
DIST (if ZEN $> 90^{o}$, $H \neq 0$)
H-HO (if ZEN $> 90^{o}$, $H \neq 0$, $N3 \neq 0$)

If a parallax correction is made, a statement reading CORRECTED FOR PARALLAX is punched between ALT and ZEN.

A brief glossary is followed by a listing of the program.

GLOSSARY

N1	number of observer input coordinates per set of ephemeris input, $1 \leq N1 \leq 99$
N2	number of output heading cards, $0 \leq N2 \leq 99$
N3	if not zero, program calculates H-HO
SIDM	sidereal time at zero hours GMT
PAR	horizontal parallax
RA	right ascention at zero hours GMT
DRA1	upper difference of right ascension
DRA0	lower difference of right ascension
DE	declination at zero hours GMT
DDE1	upper difference of declination
DDE0	lower difference of declination
GMT	Greenwich mean time
FLAT	(LAT) latitude of observer
FLONG	(LONG) longitude of observer
H	(ALT) altitude of observer
ALPHA	right ascention at specified GMT
DELTA	declination at specified GMT
SIDG	sidereal time of the Greenwich meridian
SIDL	local sidereal time
HH	hour angle
CZ	cosine of zenith angle
SZ	sine of zenith angle
CA	cosine of azimuth angle
SA	sine of azimuth angle
ZEN	zenith angle
AZIM	azimuth angle
P	radius of earth in units of the equatorial radius
R	radius of earth in kilometers at the specified latitude according to Hayford's spheroid

SHDW	shadow height = z-h csc X
HGHT	(See Figure 11)
DIST	(See Figure 11)
HHO	H-HO, z-h

```
C       ZENITH, AZIMUTH, AND MINIMUM RAY HEIGHT COMPUTATIONS
C       PROGRAMMED BY RV SILLARS
        PI=3.1415927
      1 READ92,N1,N2,N3
        IF(N2)10,5,10
     10 DO3K=1,N2
        READ99
      3 PUNCH99
      5 PUNCH20
        READ93,SIDM,PAR
        READ93,RA,DRA1,DRA0
        READ93,DE,DDE1,DDE0
        DO2I=1,N1
        READ93,GMT,FLAT,FLONG,H
        PUNCH26,GMT
        PUNCH21,FLAT
        PUNCH22,FLONG
        IF(H)9,4,9
      9 PUNCH27,H
      4 IF(DRA0)15,13,15
     13 ALPHA=RA
        DELTA=DE
        GOTO16
     15 TT=GMT/24.0
        ALPHA=RA+(DRA0+DRA1+(DRA0-DRA1)*TT)*TT/7200.0
        DELTA=DE+(DDE0+DDE1+(DDE0-DDE1)*TT)*TT/7200.0
     16 SIDC=GMT*0.0027379167
        SIDG=GMT+SIDM+SIDC
        SIDL=SIDG-FLONG
        HH=SIDL-ALPHA
        HHR=HH*0.26179939
        SHHR=SIN(HHR)
        CHHR=COS(HHR)
        PHI=FLAT*0.017453293
        SPHI=SIN(PHI)
        CPHI=COS(PHI)
        DEL=DELTA*0.017453293
        SDEL=SIN(DEL)
        CDEL=COS(DEL)
        IF(PAR)7,8,7
      7 PUNCH29
        PARR=4.8481368E-06*PAR
        SPARR=SIN(PARR)
        CP=CPHI**2+0.99327733*(SPHI**2)
        C=SQRT(1.0/CP)
        S=0.99327733*C
        PSPHI=(S+0.15677940E-03*H)*SPHI
        PCPHI=(C+0.15677940E-03*H)*CPHI
        AA=CDEL*SHHR
```

```
      BB=CDEL*CHHR-PCPHI*SPARR
      CC=SDEL-PSPHI*SPARR
      AB=SQRT(AA*AA+BB*BB)
      ABC=SQRT(AA*AA+BB*BB+CC*CC)
      SHHR=AA/AB
      CHHR=BB/AB
      SDEL=CC/ABC
      CDEL=AB/ABC
    8 CZ=SPHI*SDEL+CPHI*CDEL*CHHR
      SZ=SQRT(1.0-CZ*CZ)
      CA=(SDEL*CPHI-CDEL*SPHI*CHHR)/SZ
      SA=-CDEL*SHHR/SZ
      ZENR=ATAN(SZ/CZ)
      AZMR=ATAN(SA/CA)
      IF(CA)31,32,32
   32 IF(SA)33,34,34
   31 AZMR=AZMR+PI
      GOTO34
   33 AZMR=AZMR+2.0*PI
      GOTO34
   34 AZIM=AZMR*57.295780
      IF(CZ)37,38,38
   37 ZENR=PI+ZENR
   38 ZEN=ZENR*57.295780
      PUNCH90,ZEN
      PUNCH91,AZIM
      IF(CZ)11,2,2
   11 P1=0.99832005+0.00168349*COS(2.0*PHI)
      P2=-0.00000355*COS(4.0*PHI)+0.00000001*COS(6.0*PHI)
      P=P1+P2
      R=6378.388*P
      SHDW=R*(1.0/SZ-1.0)
      PUNCH28,SHDW
      IF(H)6,2,6
    6 HGHT=(H-SHDW)*SZ
      DIST=-(R+H)*CZ
      PUNCH94,HGHT
      PUNCH95,DIST
      IF(N3)17,2,17
   17 HHO=H-HGHT
      PUNCH96,HHO
    2 PUNCH20
      PUNCH20
      GOTO1
   92 FORMAT(3I2)
   93 FORMAT(4F10.0)
   99 FORMAT(22H
   20 FORMAT(1H )
   26 FORMAT(6H GMT =,F12.6,4H HRS)
```

```
21 FORMAT(6H LAT =,F12.6,4H DEG)
22 FORMAT(6HLONG =,F12.6,4H HRS)
27 FORMAT(6H ALT =,F12.6,4H KM )
29 FORMAT(22HCORRECTED FOR PARALLAX)
90 FORMAT(6H ZEN =,F12.6,4H DEG)
91 FORMAT(6HAZIM =,F12.6,4H DEG)
28 FORMAT(6HSHDW =,F12.6,4H KM )
94 FORMAT(6HHGHT =,F12.6,4H KM )
95 FORMAT(6HDIST =,F12.6,4H KM )
96 FORMAT(6HH-HO =,F12.6,4H KM )
   END
```

REFERENCES

1. Friedman, H., Chubb, T. A., and Siomkajlo, J. M., "A Manual on Molecular Oxygen Determination for the IQSY," in I.Q.S.Y. Instruction Manual No. 9, p. 95 (November 1964); Chubb, T. A., Friedman, H., Kreplin, R.W., Grant, R. L., and Dix, E. L.,"Preliminary Data for the Fall 1963 NRL Solar Radiation Satellite Experiment," NRL Memo Rpt. No. 1469 (November 1963).

2. Stober, A. K., "Ceramic Vacuum Ultraviolet Ion Chambers," NASA TN D-1180 (March 1962).

3. Smith, L. G. and McKinnon, P. J., "A Solar Aspect Sensor for Sounding Rockets," GCA Tech. Rpt. No. 64-12-N (July 1964).

4. Smith, L. G., Accardo, C. A., Weeks, L. H. and McKinnon, P. J., "Measurements in the Ionosphere during the Solar Eclipse of 20 July 1963," to be published in J. Atmos. Terr. Phys. (1965).

5. Stober, A. K., Scolnik, R., and Hennes, J. P., "A Vacuum Ultraviolet Photoionization Detector," Appl. Optics 2, 736 (1963).

6. Kreplin, R. W., Chubb, T. A., and Friedman, H., "X-Ray and Lyman-Alpha Emission from the Sun as Measured from the NRL SR-1 Satellite," J. Geophys. Res. 67, 2232 (1962).

7. Samson, J. A. R., "Planetary Aeronomy V: Vacuum Ultraviolet Light Sources," NASA CR-17, pp. 31-34 (September 1963).

8. Schneider, E. G., "Optical Properties of Lithium Fluoride in the Extreme Ultraviolet," Phys. Rev. 49, 341 (1936).

9. Swider, W., Jr., "The Determination of the Optical Depth at Large Solar Zenith Distances," Space Sci. 12, 761-782 (1964).

10. Ditchburn, R. W., Bradley, J. E. S., Cannon, C. G., and Munday, G., "Absorption Cross Sections for Lyman-α and Neighboring Lines," pp. 327-334 in Rocket Exploration of the Upper Atmosphere, Pergamon Press, London, (1954).

11. Lee, P., "Photodissociation and Photoionization of Oxygen (O_2) as Inferred from Measured Absorption Coefficients," J. Opt. Soc. Am. 45, 703-709 (1955).

12. Watanabe, K., "UV Absorption Processes in Upper Atmosphere," Advances in Geophysics 5, (ed. Landsberg, H. E. and Van Mieghem, J.) Academic Press, pp. 153-221 (1958).

13. Preston, W. M., "The Origin of Radio Fadeouts and the Absorption Coefficient of Gases for Light of Wavelength 1215.7Å," Phys. Rev. 57, 887-894 (1940).

14. Metzger, P. H. and Cook, G. R., "A Reinvestigation of the Absorption Cross Section of Molecular Oxygen in the 1050 to 1800Å Region," J. Quant. Spectrosc. Radiative Trans. 4, 107-116 (1964).

15. Watanabe, K. and Zelikoff, M., "Absorption Coefficients of Water Vapor in the Vacuum Ultraviolet," J. Opt. Soc. Am. 43, 753-755 (1953).

16. Ogawa, M. and Cook, G. R., "Absorption Coefficients of O_3 in the Vacuum Ultraviolet Region," J. Chem. Phys. 28, 173 (1958).

17. Bates, D. R. and Nicolet, M., "Photochemistry of Atmospheric Water Vapor," J. Geophys. Res. 55, 301 (1950).

18. Barth, C. A., "Nitrogen and Oxygen Atomic Reactions in the Chemosphere," Chemical Reactions in the Lower and Upper Atmosphere, Stanford Research Institute, Wiley & Sons, New York, 1961, pp. 303-326.

19. Carver, J. H., Mitchell, P., and Murray, E. L., "Molecular Oxygen Density and Lyman-α Absorption in the Upper Atmosphere," J. Geophys. Res. 69, 3755-3756 (1964).

20. Kupperian, J. E., Jr., Byram, E. T., and Friedman, H., "Molecular Oxygen Densities in the Mesosphere at Fort Churchill," J. Atmos. Terr. Phys. 16, 174-178 (1959).

21. Jursa, A. S., Nakamura, M., and Tanaka, Y., "Molecular Oxygen Distribution in the Upper Atmosphere," J. Geophys. Res. 68, 6145-6155 (1963).

22. Byram, E. T., Chubb, T. A., and Friedman, H., "The Dissociation of Oxygen at High Altitudes," The Threshold of Space, Pergamon Press, New York, 1957, pp.211-216.

23. Byram, E. T., Chubb, T. A., and Friedman, H., "Dissociation of Oxygen in the Upper Atmosphere," Phys. Rev. 98, 1594-1597 (1955).

24. Hinteregger, H. E., "Absorption Spectrometric Analysis of the Upper Atmosphere in the EUV Region," J. Atmos. Sci. 19, 351-368 (1962).